LA-UR -79-2070

TITLE: LASER EXCITATION OF SF_6: SPECTROSCOPY AND COHERENT PULSE PROPAGATION EFFECTS

MASTER

AUTHOR(S): C. D. Cantrell, A. A. Makarov and W. H. Louisell

SUBMITTED TO: Conference on Laser Chemistry, Ein Bokek, Israel, December 17-22, 1978

University of California

LOS ALAMOS SCIENTIFIC LABORATORY
Post Office Box 1663 Los Alamos, New Mexico 87545
An Affirmative Action/Equal Opportunity Employer

Form No. 836 R3
St. No. 2629
12/78

UNITED STATES
DEPARTMENT OF ENERGY
CONTRACT W-7405 ENG. 36

LASER EXCITATION OF SF_6: SPECTROSCOPY AND COHERENT PULSE PROPAGATION EFFECTS*

C. D. Cantrell
Theoretical Division, Los Alamos Scientific Laboratory
University of California
Los Alamos, New Mexico 87545, USA

and

A. A. Makarov
Institute of Spectroscopy, USSR Academy of Sciences
Troitzk, Podol'sky Raion
Moscow Region 142092, USSR

and

W. H. Louisell
Department of Physics
University of Southern California
Los Angeles, California 90007, USA

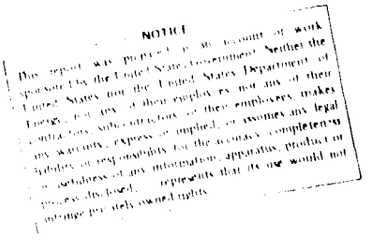

*The Los Alamos portion of this research was supported by the United States Department of Energy.

ABSTRACT

In this paper we summarize recent theoretical studies of coherent propagation effects in SF_6 and other polyatomic molecules, beginning with an account of relevant aspects of the high-resolution spectroscopy of the ν_3 band of SF_6. We show that a laser pulse propagating in a molecular gas can acquire new frequencies which were not initially present in the pulse, and that, in fact, a wave is coherently generated at the frequency of every molecular transition accessible from the initial molecular energy levels. We discuss the possible consequences of coherent generation of sidebands for the multiple-photon excitation of SF_6 and other polyatomic molecules.

I. INTRODUCTION

This paper is a brief account of recent theoretical developments in the theory of propagation of laser pulses through a molecular vapor, and of closely related topics in high-resolution molecular spectroscopy, which may help provide some insight into the role of coherence in the laser-driven multiple-photon excitation of SF_6 and other polyatomic molecules. High-resolution infrared spectroscopy and coherent propagation effects are closely linked in SF_6, both conceptually and historically. Early experimental[1-5] nd theoretical[6-9] studies of coherent propagation effects in SF_6 either suggested or depended upon specific models of the participating SF_6 energy levels and transition moments. Recent high-resolution spectroscopic studies[10-13] have provided assignments of thousands of transitions in the ν_3 fundamental of SF_6, and have helped provide a framework for the still speculative discussion[14] of excited-state transitions in SF_6. The experimental linewidth observed in saturation spectroscopy of SF_6[13] is less than 10 kHz, which we may remark appears to be inconsistent with a postulated[21] intramolecular thermalization time of 30 ps. In Part II of this paper, we shall summarize the current state of knowledge of the ν_3 fundamental ($v_3 = 0 \rightarrow v_3 = 1$) of SF_6. Although we cannot yet fully characterize the energy levels and transition moments of the states of the ν_3 mode of SF_6 with more than one vibrational quantum, we shall describe a model which we believe to possess many of the qualitative features of the energy levels and transition moments of the real SF_6 molecule.

In Part III of this paper, we shall direct most of our attention to certain coherent propagation effects which may have a major influence on the development of the spectrum of an initially monochromatic, nearly resonant laser pulse as it propagates through a vapor of polyatomic mole-

cules. Physically, the process of optical propagation consists of the creation of a coherent, macroscopic electromagnetic polarization by the incident optical electric field, and the interference of the optical electric field radiated by this macroscopic polarization with the incident field. The total field produced by this interference acts on the molecular system, and the macroscopic polarization produced thereby must be self-consistent with the total field. Such a self-consistent, nonlinear coupling is well known from Lamb's theory of the laser[22] and theories of laser pulse propagation in simplified two-level systems developed by Hopf and Scully[23] and Icsevgi and Lamb.[24] We shall summarize a general derivation[25] of the equations governing the propagation of a laser pulse interacting with an ensemble of multilevel molecular systems, within the framework of the slowly varying amplitude and phase approximation (SVAPA) and the rotating-wave approximation (RWA). We shall apply this formalism to the specific case of propagation of laser pulses in SF_6 vapor, in the limit of an optically thin sample. The coherent effects which arise in optically thin samples are optical nutation,[6] optical free induction decay[26] and photon echoes.[2,27,28] Optical nutation[6] arises from the fact that the macroscopic polarization produced by the incident optical electric field contains, in addition to the frequency ω of the incident laser field, new frequencies higher or lower than ω by an amount equal to the Rabi frequency of the transitions excited by the incident field. The macroscopic polarization then radiates a field which contains Rabi sidebands; the interference of the radiated field with the incident field makes the sidebands evident as a temporal oscillation of intensity of the total field. If a system is pumped nonresonantly by a laser pulse, the Rabi frequency is very nearly equal to the detuning, so that the frequency of one of the sidebands very

nearly coincides with the resonant transition frequency of the system. The molecular excitation produced by this nearly resonant, coherently generated field may, of course, greatly exceed the excitation which would be produced by the nonresonant incident field acting alone, depending on the magnitude of the new field coherently generated in the medium.[25,29] As is to be expected for coherent effects, the intensity of the field radiated by the macroscopic molecular polarization is proportional to the square of both the molecular number density N and the distance z traveled in the sample. Order-of-magnitude estimates presented below suggest that Rabi sidebands may well be of significant intensity for conditions often encountered in experiments on multiple-photon excitation of polyatomic molecules (pressure ~ 0.1 torr, $z \sim 10$ cm).

The major conclusion of the work summarized in this paper following our initial suggestion[29] is that the optical field coherently radiated by a molecular vapor subjected to an incident optical field contains a rich spectrum of sidebands, covering essentially the full vibration-rotation band with which the incident field interacts. The new, coherently generated field causes coherent cycling of population between the states radiatively coupled by the incident optical field. In a two-level system not subject to relaxation processes (e.g. collisions), the occurrence of coherent cycling of population would mean that, on a time scale long compared to the resonant Rabi period in the coherently generated field, approximately half the population would appear in the upper state and half in the lower state. This is a qualitatively important effect, which can greatly increase the theoretically predicted effectiveness of multiple-photon excitation of polyatomic molecules. The excitation of many rotational levels in SF_6 at surprisingly low laser intensities has been observed experimentally.[30]

It is, of course, possible to give a phenomenological interpretation of the strong excitation of many molecular energy levels not resonant with the incident laser field as being the result of rapid collisionless intramolecular energy transfer.[21] Such an intramolecular phenomenon would be completely independent of N and z, so that it should in principle be possible to distinguish unimolecular from collective coherent phenomena experimentally by a properly conducted study of the dependence of laser energy deposition in the sample (for example) on N and z. Effects due to coherent generation of Rabi sidebands should be a function of the product Nz, for optically thin samples, and for a given (fixed) incident laser intensity. It is, of course, certain that some effects of sideband generation have already been observed experimentally, but it is very easy to ascribe these effects to other causes. For example, effects due to the increase of sideband electric field as N (for fixed z) could be identified as effects of collisions among the molecules pumped by the laser. However, the effects of sideband generation will also depend on z (for fixed N), and are thus distinguishable in principle from collisional effects.

Although we are aware that the ideas about coherent propagation effects described in this paper are at odds with some published concepts of multiple-photon excitation, we are hopeful that our work will at least stimulate new experiments, and new interpretations of already published data.

II. HIGH-RESOLUTION SPECTROSCOPY OF THE ν_3 BAND OF SF_6

In this section we shall summarize the current state of high-resolution spectroscopy of the ν_3 fundamental band ($v_3 = 0 \rightarrow v_3 = 1$) of SF_6, and shall indicate some current ideas on the structure of SF_6 states with two or more ν_3 quanta. The spectra of the infrared-active modes of tetrahedral and octahedral spherical-top molecules are highly complex, owing in large part to the fact that these vibrational modes are triply degenerate. In octahedral spherical-top molecules, the two triply-degenerate infrared-active modes, ν_3 and ν_4, both belong to the (three-dimensional) F_{1u} representation of the octahedral point group O_h (Fig. 1). The ν_3 mode in SF_6 involves primarily stretching motions, while the ν_4 mode involves both stretching and bending motions.[31] The complexity of the vibration-rotation spectra of these triply-degenerate modes is the result of many physical effects: (a) splitting of levels with two or more vibrational quanta by vibrational anharmonic effects; (b) Teller Coriolis splitting (and Coriolis interaction between different vibrational states) due to interactions between vibrational and rotational angular momenta; (c) splitting of each rotational level (which is (2J+1)-fold degenerate in the molecule-fixed field frame) into as many states as are allowed by the molecular point-group symmetry, due to tensor vibration-rotation interactions; (d) nuclear hyperfine splitting. All of these effects are significant in understanding and assigning the experimentally observed high-resolution spectra of the SF_6 ν_3 band. Even the nuclear hyperfine splitting has been resolved, and some additional vibration-rotation spectroscopic constants determined, in recent sub-Doppler studies of SF_6.[13]

However, essentially nothing is firmly established with regard to the spectroscopic constants of states in SF_6 with two or more vibrational quanta. In view of this fact, all we can attempt in this brief review with regard to vibrational overtone states is to outline a model which possesses some important qualitative features of the overtone states and excited-state transition moments of the real SF_6 molecule. The model we shall outline, which has the virtues of computational convenience and physical reasonableness, has been used in the numerical studies of coherent propagation effects in SF_6 which we shall describe in Section III of this paper.

The derivation of the quantum-mechanical Hamiltonian for a vibrating, rotating polyatomic molecule has been the subject of discussion and study for many years; we refer the reader to a small subset of the literature for a detailed summary.[32-35] A full derivation of the effective vibration-rotation Hamiltonian for a single (degenerate) mode of a spherical-top molecule, starting with a power-series expansion of the vibration potential energy, involves a sequence of contact transformations to bring operators of successively higher order to approximately diagonal form. Such a transformation has been carried out for a triply-degenerate mode of a tetrahedral molecule,[36] but has not yet been attempted in the octahedral case. An alternative approach which is very useful for the assignment of spectra and the determination of spectroscopic constants is to expand the vibration-rotation Hamiltonian in terms of all operators (up to a given order in the vibrational normal coordinates, vibrational and rotational angular momenta, etc.) which are allowed by the molecular symmetry group.[37] The phenomenological constants which multiply the different operators appearing in such an expansion can, of course, be expressed in terms of the parameters charac-

terizing the molecular force field, the equilibrium moment of inertia, etc., and such expressions are known for the tetrahedral case.[38] Because of the far greater complexity of the vibrational Hamiltonian for octahedral molecules,[39] only the phenomenological approach of regarding the constants which appear in the vibration-rotation Hamiltonian as independent parameters, and adjusting these parameters to give a least-squares fit to experimentally measured spectral line positions, has been followed for SF_6 and other octahedral molecules.[10-12]

The amount of spectroscopic detail which can usefully be studied theoretically depends to a great extent on the degree of resolution which can be achieved experimentally. Grating spectra[40] of SF_6 at room temperature show a smooth band contour uninterrupted by rotational structure. A grating spectrum of SF_6 at a temperature of 153K[41] (Fig. 2), at which 80% of the SF_6 molecules are in the vibrational ground state, shows an irregular contour which is not noise, but is also not recognizable as rotational structure. A real understanding of the SF_6 spectrum depended on obtaining experimental spectra with a resolution limited only by the SF_6 Doppler width (30 MHz at room temperature). The application of semiconductor diode lasers to vibration-rotation spectroscopy[42-44] resulted in Doppler-limited spectra of SF_6 covering a frequency range of approximately ±1 GHz near the CO_2 laser lines overlapping the SF_6 ν_3 band.[45] Although these spectra went unassigned at that time, they proved to be very useful later[10-12] owing to the fact that they had been calibrated by heterodyning the tunable semiconductor diode laser with a fixed-frequency CO_2 laser stabilized at the center of the CO_2 laser line.[45] This technique gives a direct measurement of the frequency difference between the center of the CO_2 laser line and the spectroscopic feature to which the semiconductor

diode laser is tuned, and is thus considerably superior in accuracy to the technique of calibration by etalon fringes which is more commonly used in laser diode spectroscopy.[46] Much greater accuracy can now be achieved by sub-Doppler saturation spectroscopy[13] than by heterodyne calibration of Doppler-limited spectra.

Assignment of the SF_6 ν_3 band[10-13] was made possible by Doppler-limited spectra covering a large range near the ν_3 band center,[47] (Fig. 3) in SF_6 at temperatures where more than 90% of the SF_6 molecules are in the ground vibrational state, and by knowledge of the nuclear spin-statistical weights[48,49] which made it possible to recognize the pattern or "fingerprint" of fine-structure lines associated with each value of the total angular momentum J. At first only the ν_3 P and R branches could be assigned;[10] later the Q branch was also assigned[11] (Fig. 4). More recently, saturation spectroscopy of the ν_3 band of SF_6 has made it possible to determine a more accurate set of vibration-rotation spectroscopic parameters, and to uncover effects of nuclear hyperfine splitting.[13]

Prior to the publication of the assignment of the ν_3 band of SF_6, a number of studies of coherent propagation effects suggested, or depended upon, certain qualitative aspects of the spectroscopy of the ν_3 band. Observations of optical nutation[3,5] were interpreted to give rather different values of the ν_3 transition dipole moment, one of which[5] compared favorably with later determinations based on the ν_3 band strength[50] and the intensity of single lines in the high-resolution spectrum.[51] Self-induced transparency[52] was inferred to occur in SF_6 irradiated by a pulsed CO_2 laser;[1] although some details of the process of inference were not in agreement with theoretical predictions for two-level systems,[7] self-induced transparency was later unambiguously observed[3] in SF_6 ir-

radiated by some (but not all) of the CO_2 laser lines overlapping the SF_6 ν_3 band (Table I). At first it was argued that self-induced transparency (and coherent propagation effects in general) could occur in SF_6 only if the value of the total angular momentum of the initial state were very low. It was later shown theoretically[8,9] that coherent propagation effects can occur even for very high values of J, because of a "clustering" of the transition moments for different initial values of the spatial quantum number M. We shall discuss this point in greater detail below, after deriving the form of the transition moments for a spherical-top molecule. Experimental and theoretical studies[2,28] of photon echoes in SF_6 have led to incomplete agreement between the observed and predicted relationship between the pump polarizations and the echo polarization. Finally, infrared-infrared double resonance experiments[53-55] and shock-tube studies of the SF_6 absorption contour[56] gave important semiquantitative information on the magnitude of SF_6 J values for states interacting with the various CO_2 laser lines. More recent double-resonance studies of SF_6 have provided data which challenge theoretical efforts at assignment.[20,57]

Vibration-Rotation Basis

The vibration-rotation basis states for a spherical-top molecule may conveniently be taken as linear combinations of products of vibrational wavefunctions and rotational wavefunctions, within the framework of the Born-Oppenheimer approximation. Two vibration-rotation bases which are widely used in the theory of spherical-top molecules employ vibrational wavefunctions $\phi_m^{v\ell}$ which are adapted to spherical symmetry, and rigid-rotor wavefunctions D_{KM}^J. In the coupled spherical basis,[38] a linear combination of the products $D_{KM}^J \phi_m^{v\ell}$ is taken which results in coupled angular-momentum basis functions $\Phi_{K\ M}^{v\ell JR}$. In the symmetry-adapted basis introduced by Moret-

Bailly,[58] a different linear combination of the products $D^J_{KM}\,\phi^{v\ell}_m$ is taken, such that the sum belongs to one row of an irreducible representation of the molecular point group. Both of these bases are important for a discussion of spherical-top energy levels and transition moments.

The vibrational wavefunctions $\phi^{v\ell}_m$ in the spherical basis are eigenfunctions of the total number of vibrational quanta (v), the vibrational angular momentum (ℓ = v, v-2, ..., 1 or 0) and the projection of the vibrational angul r momentum along the molecule-fixed z axis (m = $-\ell$, $-\ell+1$, ..., ℓ). Explicitly, as functions of the normal coordinates q_1, q_2, q_3 of a triply-degenerate vibrational mode, they are[59]

$$\phi^{v\ell}_m = N_{v\ell}\, Y_{\ell m}(\vec{q}/|\vec{q}|)e^{-q^2/2}\,(q^2)^{\ell/2}\, L^{(\ell+\frac{1}{2})}_{\frac{1}{2}(n-\ell)}\,(q^2) \tag{1}$$

where

$$q^2 = \sum_{j=1}^{3} q_j^2 = |\vec{q}|^2 \tag{2}$$

$$\vec{q} = (q_1, q_2, q_3) \tag{3}$$

$$N_{v\ell} = \{2[\tfrac{1}{2}(v-\ell)]!\}^{\frac{1}{2}}\,\{[\tfrac{1}{2}(v+\ell+3)]!\}^{-\frac{1}{2}} \tag{4}$$

and where $Y_{\ell m}$ is a spherical harmonic; $L^{(\alpha)}_p$ is an associated Laguerre polynomial.[60]

The rigid-rotor wavefunctions for a given total angular momentum J, with the projection of J along the molecule-fixed axis and space-fixed axis being, respectively, K and M, are proportional to the elements of the representation ' of the rotation group,

$$\psi^{J}_{KM} = \left[\frac{2J+1}{8\pi^2}\right]^{\frac{1}{2}} D^{J}_{KM}\ (\Omega^{-1}) \tag{5}$$

where Ω is the 3×3 matrix which rotates the components of a vector in the laboratory-fixed frame into the components of the same vector in the molecule-fixed frame:

$$\vec{x}_{mol} = \Omega\vec{x}_{lab} \ . \tag{6}$$

Eq. (5) is a direct consequence of the symmetry of a spherical-top molecule, and may be established by purely group-theoretical arguments.[61,62]

The coupled spherical vibration-rotation basis vectors are

$$\Phi^{v\ell JR}_{K_R M} = \sum_{m} \langle \ell J; mK | RK_R \rangle \ [\phi^{v\ell}_{m}]^{*} \ \psi^{J}_{KM} \tag{7}$$

where $K_R = K-m$. To obtain (7) one must <u>subtract</u> the vibrational angular momentum $\vec{\ell}$ from the total angular momentum $\vec{J}$ to obtain the purely rotational angular momentum of the molecular framework:

$$\vec{R} = \vec{J} - \vec{\ell} \ . \tag{8}$$

The symmetry-adapted basis functions are eigenfunctions of the rotational angular momentum R, and the laboratory-fixed z component of total angular momentum M, and also belong to a specific row of a specific irreducible point-group representation. The symmetry-adapted basis may be obtained[58,64] from the coupled spherical basis by a unitary transformation matrix $^{(R)}G$:

$$\psi^{v\ell JR}_{pM} = \sum_{K_R} {}^{(R)}G_{p}^{K_R} \ \Phi^{v\ell JR}_{K_R M} \tag{9}$$

In (9), the indices

$$C = (\Gamma\gamma) \quad \text{and} \quad p = c^{(n)} \tag{10}$$

are composite labels consisting of the irreducible representation Γ, the row γ of that representation, and an index n which distinguishes the different state vectors with the same point-group symmetry which arise in the reduction of D^R into irreducible representations of the molecular point group. The elements of $^{(R)}G$ have been calculated for R up to 130,[64,65] and are tabulated[58] for $R \leq 20$.

Vibration-Rotation Hamiltonian

It was shown in the pioneering work of Hecht,[38] Moret-Bailly[65] and Louck[66] that many advantages accrue from expressing the vibration-rotation Hamiltonian for a spherical-top molecule in terms of spherical tensor operators. The greatest advantage is that the Racah-Wigner angular momentum calculus allows one to take the coupled-basis matrix elements of the qth component $T_q^{(k_1k_2k)}$ of a spherical tensor operator $T^{(k_1k_2k)}$ of rank k (formed by coupling a purely vibrational tensor operator $T_{vib}^{(k_1)}$ of rank k_1 to a purely rotational operator $T_{rot}^{(k_2)}$ of rank k_2) in a completely systematic manner:

$$(\Phi_{K_R'M'}^{v'\ell'JR'},\ T_q^{(k_1k_2k)}\ \Phi_{K_RM}^{v\ell JR})$$

$$= \delta_{M'M}(-1)^{R+K_R'} \begin{pmatrix} R & k & R' \\ K_R & q & -K_R' \end{pmatrix} [(2k+1)(2R+1)(2R'+1)]^{\frac{1}{2}} \tag{11}$$

$$\cdot \begin{Bmatrix} \ell' & \ell & k_1 \\ J & J & k_2 \\ R' & R & k \end{Bmatrix} \langle v'\ell'||T_{vib}^{(k_1)}||v\ell\rangle\langle J||T_{rot}^{(k_2)}||J\rangle$$

Only the reduced matrix elements need to be evaluated (once!) by a calculation involving the explicit forms of the operators $T_{vib}^{(k_1)}$ and $T_{rot}^{(k_2)}$. The reduced matrix elements needed for most operators in the SF_6 vibration-rotation Hamiltonian are tabulated by Hecht[38] and Robiette et al.[67]

To construct a vibration-rotation Hamiltonian which is invariant under the operations of the molecular point group, it is in general necessary to form linear combinations of the spherical tensor components $T_q^{(k_1k_2k)}$. In fact, the octahedrally (or tetrahedrally) invariant linear combinations are

$$T_{A_1}^{(k_1k_2k)} = \sum_q (k)G_{A_1}^q \; T_q^{(k_1k_2k)} \tag{12}$$

where A_1 is the totally symmetric representation of the point group. In terms of the symmetry-adapted basis (9), we can use (12) to reduce (11) to the form

$$(\psi_{p'M'}^{v'\ell'JR'}, \; T_{A_1}^{(k_1k_2k)} \; \psi_{pM}^{v\ell JR})$$

$$= \delta_{MM'} \begin{Bmatrix} \ell' & \ell & k_1 \\ J & J & k_2 \\ R' & R & k \end{Bmatrix} [(2k+1)(2R+1)(2R'+1)]^{\frac{1}{2}}$$

$$\cdot \langle v'\ell'||T_{vib}^{(k_1)}||v\ell\rangle \langle J||T_{rot}^{(k_2)}||J\rangle (-1)^R \; F_{A_1p'p}^{(kR'R)} \tag{13}$$

where the Moret-Bailly $F^{(k)}$ coefficient[58] is defined as

$$F_{A_1p'p}^{(kR'R)} = \sum_{m_1m_2m_3} (k)G_{A_1}^{m_1} \; (R')G_{p'}^{m_2} \; (R)G_p^{m_3} \begin{pmatrix} R' & k & R \\ m_2 & m_1 & m_3 \end{pmatrix} \tag{14}$$

The off-diagonal ($R' \neq R$) $F^{(4)}$ and $F^{(6)}$ coefficients have been calculated numerically by Krohn[xx] for $R' \leq 98$, $R \leq 98$, and the diagonal ($R' = R$) $F^{(4)}$ and $F^{(6)}$ coefficients have been calculated[64] for $R \leq 120$.

In agreement with Robiette et al.,[67] we adopt the following notation for the tensor operators appearing in the vibration-rotation Hamiltonian:

$$T^{mn}_{k_1 k_2 k;q} = (\hat{n})^m \, (\hat{J}^2)^n \, T^{(k_1 k_2 k)}_q \tag{15}$$

where $\hat{n}$ is the operator giving the total number of ν_3 vibrational quanta. In this notation, the vibration-rotation Hamiltonian for the ν_3 mode of SF_6 including all allowed operators up to and including rank $k = 6$, is shown in Table I. The matrix elements of this Hamiltonian may be calculated using (11) or (13) (or using other bases), and the Hamiltonian may be diagonalized numerically.

Fitting of Spectroscopic Parameters

It is evident from (11) or (13) that the Hamiltonian will, in general, not be diagonal in the rotational angular momentum R. For not too large values of J (in SF_6, for $J \lesssim 25$) the off-diagonal elements in (13) lead to negligible effects on the energy eigenvalues. In that case the diagonal contribution to the energy eigenvalue $E^{v\ell JR}_{pM}$ of a particular tensor operator may be written down directly from (13). Evaluation of the 9J symbols and reduced matrix elements for the operators appearing in Table I leads to the parametrization of the fundamental transition frequencies

$$\begin{aligned}
\nu_R(R,p) &= E^{1,1,R+1,R}_{pM} - E^{0,0,R,R}_{pM} \quad \text{(R branch, } J \rightarrow J+1\text{)} \\
\nu_Q(R,p) &= E^{1,1,R,R}_{pM} - E^{0,0,R,R}_{pM} \quad \text{(Q branch, } J \rightarrow J\text{)} \\
\nu_p(R,p) &= E^{1,1,R-1,R}_{pM} - E^{0,0,R,R}_{pM} \quad \text{(P branch, } J \rightarrow J-1\text{)}
\end{aligned} \tag{16}$$

TABLE I.

VIBRATION–ROTATION HAMILTONIAN FOR A TRIPLY DEGENERATE MODE

(K. T. Hecht, J. Mol. Spectrosc. 5, 355 (1960); A. G. Robiette, D. L. Gray and F. W. Birss, Mol. Phys. 32, 1591 (1976))

$$H = \omega_s T^{10}_{000} + B_0 T^{02}_{000} - 2B\zeta_s T_{110} + G_{ss} \vec{\ell}^{\,2}_s + T_{ss} T_{404}$$

$$- \alpha T^{11}_{000} + \alpha_{220} T_{220} + \alpha_{224} T_{224}$$

$$- D_0 T^{02}_{000} - D_{t0} T_{044} + F_{110} T^{01}_{110} + F_{134} T_{134}$$

$$- (D\text{-}D_0) T^{12}_{000} - (D_t - D_{t0}) T^{10}_{044} + G_{220} T^{01}_{224}$$

$$+ G_{244} T_{244} + G_{246} T_{246}$$

$$+ H T^{03}_{000} - H_{4t} T^{01}_{044} + H_{6t} T_{066}$$

TABLE II.

BOBIN–FOX PARAMETRIZATION OF SPHERICAL–TOP TRANSITION FREQUENCIES

- NOTATION: R = ROTATIONAL ANGULAR MOMENTUM
  p = OCTAHEDRAL OR TETRAHEDRAL SYMMETRY SPECIES AND INDEX
  $F^{(kRR)}_{A_1pp}$ = NORMALIZED EIGENVALUE OF DIAGONAL BLOCK OF HAMILTONIAN (MORET-BAILLY) INCLUDING OPERATORS OF RANK k IN R
  M = −R(P BRANCH) OR R+1 (R BRANCH)
  $\Delta(R,p)$ = OFF-DIAGONAL CORRECTION (IN R)

- P AND R BRANCHES:

$$\nu_{P,R}(R,p) = m + nM + pM^2 + qM^3 + sM^4 + tM^5 + xM^6$$
$$+ (g - hM + kM^2 + \ell M^3 + jM^4)\frac{(-1)^R}{D,F(R)} F^{(4RR)}_{A_1pp}$$
$$+ (z' + z''M + z'''M^2)\frac{(-1)^R}{D',F'(R)} F^{(6RR)}_{A_1pp}$$
$$+ \Delta_{P,R}(R,p)$$

- Q BRANCH

$$\nu_Q(R,p) = m + vR(R+1) + w[R(R+1)]^2$$
$$+ \left|-2g + uR(R+1) + z[R(R+1)]^2\right| \frac{(-1)^R}{E(R)} F^{(4RR)}_{A_1pp}$$
$$+ [-2z' + z'''R(R+1)]\frac{(-1)^R}{E'(R)} F^{(6RR)}_{A_1pp}$$
$$+ \Delta_Q(R,p)$$

TABLE II (cont.)

FUNCTIONS APPEARING IN BOBIN–FOX PARAMETRIZATION

$$D(R) = \frac{2R\ (2R-1)}{[(2R-3)\ \cdots\ (2R+5)\ ]^{1/2}}$$

$$D'(R) = \frac{2R\ (2R-1)}{[(2R-5)\ \cdots\ (2R+7)\ ]^{1/2}}$$

$$E(R) = \frac{(2R+2)\ (2R+3)}{[(2R-3)\ \cdots\ (2R+5)\ ]^{1/2}}$$

$$E'(R) = \frac{(2R+2)\ (2R+3)}{[(2R-5)\ \cdots\ (2R+7)\ ]^{1/2}}$$

$$F(R) = \frac{2R\ (2R+2)}{[(2R-3)\ \cdots\ (2R+5)\ ]^{1/2}}$$

$$F'(R) = \frac{2R\ (2R+2)}{[(2R-5)\ \cdots\ (2R+7)\ ]^{1/2}}$$

shown in Table II.[68] These expressions have been extensively used in fitting Doppler-limited spectra of SF_6[10-12]. The relationship between the Hamiltonian parameters appearing in Table I and the spectroscopic parameters appearing in Table II is complex, and will be discussed in a future publication.[70] Also, in Table II, the quantities $\Delta_P(R,p)$, $\Delta_Q(R,p)$, and $\Delta_R(R,p)$ are, by definition, the difference between the transition frequencies determined through exact diagonalization of the Hamiltonian including matrix elements off-diagonal in R, and the transition frequencies calculated using approximate energies calculated using the purely diagonal (in R) form of (13).

The assignment of an actual spectrum falls into three stages: (a) provisional assignment, using approximate parameters obtained by a hand calculation, etc.; (b) determination of preliminary constants given a provisional assignment; (c) assignment of additional lines and final determination of constants. Stages (a) and (b) may be accomplished using the modified Bobin-Fox parametrization[68] shown in Table II, with $\Delta_{P,Q,R}(R,p) = 0$. The values of $\Delta_{P,Q,R}(R,p)$ may then be determined by an exact diagonalization (including matrix elements off-diagonal in R) using the parameters determined in (b). The resulting numerically determined values of $\Delta_{P,Q,R}(R,p)$ may be inserted in the modified Bobin-Fox expressions (Table II), new constants determined, and so on until the iteration converges on a consistent set of parameters.[10-12] The values and standard deviations of the SF_6 spectroscopic parameters obtained using line positions measured by high-resolution saturation spectroscopy are shown in Table III.[13]

In Fig. 5 we show a saturation spectrum[13] of a portion of the frequency interval (near the P(16) CO_2 laser line[70] at 947.7417363 cm^{-1}) included at lower resolution in Figs. 3 and 4. The positions of the lines marked with a bullet in Fig. 5 were measured by the technique of frequency offset locking[71] to an accuracy of a few kHz (with respect to the reference CO_2 laser line). The total tuning range in Fig. 5 is approximately ±250 MHz. The experimental linewidth is less than 10 kHz.

Transition Moments

To complete our survey of spherical-top spectroscopic theory, we give a brief derivation of the transition moments for dipole-allowed transitions in which one vibrational quantum changes, in the bases (7) and (9).[72-75] The spherical components of the dipole transition operator in the laboratory-fixed frame, μ_σ, are physically the quantities which interact with an externally applied optical electric field E, through the dipole Hamiltonian. Consequently we shall calculate the matrix elements of the laboratory-fixed components μ_σ, which are related to the molecule-fixed components of the vibrational normal coordinates by the equation

$$\mu_\sigma = A \sum_\tau D^1_{\tau\sigma}(\Omega^{-1}) q_\tau \ , \tag{17}$$

where A is a constant characteristic of the vibrational mode. For an individual with extensive experience in tensor operators it is easy to see from (17) that the dipole operator is of tensor form, with $k_1 = 1$, $k_2 = 1$, and $k = 0$, so that the matrix elements follow directly from (11) or (13). A more pedestrian approach is the following:[74,75] express the states $\Phi^{v\ell JR}_{K\ M}$ using (7); use the Wigner-Eckart theorem to evaluate $(\phi^{v'\ell'}_{m'}, q_\tau \phi^{v\ell}_m)$; evaluate the rotational matrix elements using the well-known integral over a product of three D^J's; and resum all the resulting 3J symbols

to 6J or 9J symbols. The results are[73-75]

$$(\Phi_{p'M'}^{v'\ell'J'R'}, \mu_\sigma \Phi_{pM}^{v\ell JR})$$

$$= A\delta_{RR'} \cdot \delta_{pp'} \cdot (-1)^{J+M'+1} \begin{pmatrix} J & 1 & J' \\ M & \sigma & -M' \end{pmatrix}$$

$$\cdot [3(2R+1)(2J+1)(2J'+1)]^{\frac{1}{2}} \langle v\ell||q||v'\ell' \rangle$$

$$\cdot \begin{Bmatrix} \ell' & \ell & 1 \\ J' & J & 1 \\ R' & R & 0 \end{Bmatrix} \tag{18}$$

The reduced matrix element is

$$\langle v\ell||q||v'\ell' \rangle = \begin{cases} [(v+\ell+3)(\ell+1)/2]^{\frac{1}{2}} & \text{when } v' = v+1, \ \ell' = \ell+1 \\ [(v-\ell+2)\ell/2]^{\frac{1}{2}} & \text{when } v' = v+1, \ \ell' = \ell-1 \end{cases} \tag{19}$$

The selection rules evident from (19) are:

$$R' = R \tag{20}$$

$$p' = p \tag{21}$$

$$v' = v \pm 1 \tag{22}$$

$$\ell' = \ell \pm 1 \tag{23}$$

$$J' = J \text{ or } J \pm 1 \tag{24}$$

$$M' = M + \sigma \tag{25}$$

Selection rules (22) and (23) are expected to hold for all dipole-allowed infrared transitions; physically they imply that one vibrational quantum is changed in the transition. Selection rules (20) and (21) are applicable

only when the functions $\Phi_{pM}^{v\ell JR}$ are nearly eigenfunctions of the exact Hamiltonian. However, several of the tensor operators in Table I, including the possibly important vibrational anharmonic operator T_{404}, mix states with different R. When this happens, (20) no longer applies. Also, the nuclear hyperfine interaction mixes states with different point-group symmetry type p (particularly in the ground vibrational state[13]), so that (21) is also an approximate selection rule. Transitions which do not obey the selection rules (20)-(21) may have a substantial effect on the process of multiple-photon excitation,[76] through nearly resonant enhancement of multiphoton transitions. It is not clear that transitions which violate (20)-(21) are necessarily orders of magnitude weaker than transitions which obey (20)-(21), since the mixture of states with different values of R and p need not be negligible.

It should be noted from (18) that the transition moment is always proportional to the 3J symbol

$$\begin{pmatrix} J & 1 & J' \\ M & \sigma & -M' \end{pmatrix} \tag{26}$$

regardless of the mixture of states produced by the vibration-rotation interaction. (If the nuclear hyperfine interaction is strong, J and M must be replaced by F and M_F.) The presence of the 3J symbol in (18) is a direct consequence of spherical symmetry.

A Model for the ν_3 Mode of SF_6

In this work we have dedicated ourselves to a study of coherent effects in multiple-photon excitation, and to an investigation of whether processes which in the past have been ascribed to unimolecular or collisional relaxation are in fact the result of coherent processes. The details of our model are conditioned by this physical approach. We assume that the mole-

cule remains in the v_3 vibrational mode, i.e. that there is no intramolecular relaxation of population. In this case the basic physics of the interaction of a single molecule with a laser field is multiphoton excitation.[77-80] The molecule goes from $v_3 = 0$ to $v_3 = N$ by absorption of N photons, without necessarily making resonant single-photon transitions along the way. The resonant laser frequency for an N-photon transition from $v_3 = 0$ to $v_3 = N$ is given by

$$\omega_{pM}^{N\ell JR} = N^{-1} \left[E_{pM}^{N\ell JR} - E_{pM}^{0,0,R,R}\right] \tag{27}$$

As the proliferation of indices in (27) indicates, there are many nearby N-photon resonances (for all the allowed values of ℓ,J,R, and p) with a wide range of resonant frequencies. The population which can be excited to $v_3 = N$ in an N-photon resonance can, in principle, be large; the highest and lowest levels can engage in coherent Rabi oscillations, much like the upper and lower levels of a two-level system. If levels between $v_3 = 0$ and $v_3 = N$ are also significantly excited (due to a near-coincidence of $\omega_{pM}^{N\ell JR}$ with one or more single-photon transition frequencies, for example) then the analogy with a two-level system is no longer applicable, but the total number of molecules excited from $v_3 = 0$ may be higher. Certain physical effects can, in fact, lead to a high probability of coincidence of single-photon transition frequencies with multiphoton resonant frequencies, and thereby compensate the expected anharmonic decrease of the transition frequencies from v_3 to v_3+1 with increasing v_3. Both rotational energy[77,81] and vibrational anharmonic splitting[14] can at least partially compensate the effects of vibrational anharmonicity on single-photon transition frequencies. Both of these effects are present in our model. We have included rotations by including the terms

$$BT^{01}_{000} - 2B\zeta_3\, T_{110} = B\vec{J}^2 - 2B\zeta_3\, \vec{J}\cdot\vec{\ell} \tag{28}$$

from the first line of Table II. Anharmonic splitting is provided in our model by the spherically symmetric anharmonic contribution

$$G_{33}\, \vec{\ell}_3^{\,2} \tag{29}$$

from Table II. We have neglected the octahedrally symmetric anharmonic contribution

$$T_{33}\, T_{404} \tag{30}$$

in Table II, which also produces anharmonic splitting, because this term couples states $\Psi^{v\ell JR}_{pM}$ with different values of ℓ (and R) and thereby complicates the model. Neglecting (30) entails a neglect of transitions which violate selection rule (20).

In our numerical calculations we at first[82] lumped together in a single "effective state"[83] $|v\ell JR\rangle$ all the states $\Psi^{v\ell JR}_{pM}$ with given (fixed) values of v, ℓ, J and R. This reduces the number of states involved in the computations, but forces one to employ instead of (18) a "typical" transition moment, which we take to be the root mean square of (18):

$$\langle v'\ell'J'R'|\mu|v\ell JR\rangle_{typ}$$

$$= A\, \langle v\ell||q||v'\ell'\rangle\, W(\ell'\ell J'J;1R) \tag{31}$$

where W is a Racah coefficient. In other words, this approach makes a simplification in assuming that both energy levels and transition moments are independent of p and M.

In more recent computations we have employed the effective states $|v\ell JR;M\rangle$, in which states with different octahedral symmetry types (p) but the same quantum numbers v, ℓ, J, R and M are lumped together. In this

case the state-to-state transition moments (18), which are independent of p, must be used. The approximation made in this case is to neglect the dependence of the energy levels on p; i.e. we neglect the vibration-rotation fine structure. In both cases we have, of course, also neglected the effects of nuclear hyperfine effects, which would mix states with different symmetry type p; these are already lumped together in our effective-states approaches.

IV. COHERENT PROPAGATION EFFECTS IN SF_6

Electromagnetic Field Equations

We consider an infinite plane, quasimonochromatic electromagnetic wave traveling in the +z direction, with a real electric field

$$\vec{E} = \hat{e}E(z,t) \ , \tag{32}$$

to be incident on a uniform gaseous medium with molecular number density N. In (32), $\hat{e}$ is a unit polarization vector, such that

$$\hat{e}^* \cdot \hat{e} = 1 \ . \tag{33}$$

The incident field sets up a polarization density

$$\vec{P} = \hat{e}P(z,t) \ . \tag{34}$$

The propagation of $\vec{E}$ in the medium is described by the one-dimensional wave equation (in MKS units)

$$\frac{\partial^2 E}{\partial z^2} - \frac{1}{c^2}\frac{\partial^2 E}{\partial t^2} + \frac{c\kappa}{2}\frac{\partial E}{\partial t} = -\mu_0 \frac{\partial^2 P}{\partial t^2} \ . \tag{35}$$

In (35), κ is a linear attenuation coefficient introduced to allow for scattering losses, etc. In order to make further progress, we make the slowly varying amplitude and phase approximation (SVAPA): we assume that the field and polarization are of the form

$$E(z,t) = E'(z,t) \cos \zeta(z,t) \tag{36}$$

$$P(z,t) = C(z,t) \cos \zeta(z,t) + S(z,t) \sin \zeta(z,t) \tag{37}$$

$$\zeta(z,t) = kz - \omega t + \phi(z,t) \tag{38}$$

where E', C, S, and ϕ are slowly varying in the sense that

$$\left|\frac{\partial f}{\partial z}\right| << |kf| \ , \ \left|\frac{\partial f}{\partial t}\right| << |\omega f| \tag{39}$$

where f is E′, C, S or ϕ. If we insert (36)-(38) in (35), and make the SVAPA (39), then we find that

$$\left[\frac{\partial}{\partial z} + \frac{1}{c}\frac{\partial}{\partial t} + \frac{\kappa}{2}\right]\mathcal{E} = \frac{k}{2\varepsilon_0}\mathcal{P} \tag{40}$$

where we have introduced the complex electric field

$$\mathcal{E}(z,t) = E'(z,t)e^{i\phi(z,t)} \tag{41}$$

and complex polarization density

$$\mathcal{P}(z,t) = [S(z,t) + iC(z,t)]e^{i\phi(z,t)} \ . \tag{42}$$

In terms of the retarded-time variables

$$z' = z \ , \quad t' = t - z/c \tag{43}$$

(40) becomes

$$\left[\frac{\partial}{\partial z'} + \frac{\kappa}{2}\right]\mathcal{E} = \frac{k}{2\varepsilon_0}\mathcal{P} \ . \tag{44}$$

As it stands Eq. (44) is simply an approximate form of Maxwell's equations adapted to a particular physical situation, and is therefore incomplete. To complete (44) we must give a prescription for calculating $\mathcal{P}$, which we shall do below. In general $\mathcal{P}$ depends on $\mathcal{E}$ in a highly nonlinear manner, so that (44) is one of a set of coupled, nonlinear partial differential equations. A self-consistent solution of these equations can ordinarily be obtained only by numerical calculations.

Calculation of the Polarization Density

The polarization in a dilute medium is simply the product of the molecular number density N and the quantum-mechanical expectation value of the dipole operator:

$$P = N\ \mathrm{tr}(\rho\vec{\mu}\cdot\hat{e}^{*}) = N\ \mathrm{tr}(\rho\mu_{\sigma}) \ . \tag{45}$$

where ρ is the reduced density matrix for the ν_3 mode of SF_6.[84] In terms of a basis of states $|vA\rangle$, where v is the vibrational quantum number and A denotes the remaining quantum numbers, (45) becomes

$$P = \sum_{v,u} \sum_{A,B} \rho_{vA,uB}\ \mu_{vA,uB} \ . \tag{46}$$

In keeping with the SVAPA, which removes harmonics from Maxwell's equations, we shall employ the rotating-wave approximation (RWA), which removes harmonics from the equation of motion for the density matrix ρ. Let

$$\rho_{vA,uB} = e^{i(\Omega_u - \Omega_v)t'}\ \tilde{\rho}_{vA,uB} \tag{47}$$

where

$$\Omega_v = v\omega \ . \tag{48}$$

Since $-\omega t' = kz-\omega t$ by (43),(47) removes the rapid spatial and temporal oscillation of ρ created by the incident field. The equation of motion for ρ is[84]

$$\frac{\partial \rho_{vA,uB}}{\partial t}$$

$$= \{-\frac{i}{\hbar}(E^{vA} - E^{uB}) - \gamma_{vA,uB}(1 - \delta_{vu}\delta_{AB})\}\rho_{vA,uB}$$

$$- \frac{i}{\hbar} E(z,t) \sum_{qC} [\mu_{vA,qC}\rho_{qC,uB} - \rho_{vA,qC}\mu_{qC,uB}]$$

$$- \delta_{uV}\delta_{AB} \sum_{qC} [\rho_{vA,vA} w_{vA,qC} - \rho_{qC,qC} w_{qC,vA}] \qquad (49)$$

where $\gamma_{vA,uB} = \gamma_{uB,vA}$ is the dephasing rate of an off-diagonal density-matrix element and $w_{vA,uB}$ is the rate of population transfer (per molecule) from vA to uB. For a two-level system, the relationship between the γ's and w's and the more familiar relaxation constants T_1 and T_2 is

$$(T_1)^{-1} = \frac{1}{2}(w_{12} + w_{21}) \qquad (50)$$

$$(T_2)^{-1} = \gamma_{12} = \gamma_{21} \cdot \qquad (51)$$

We regard the physical origin of the γ's and w's as collisions, not intramolecular transitions.

We implement the RWA by substituting (47) into (49), using (36), (41) and (48), and discarding terms which vary as $\exp(\pm 2i\omega t')$. The result is

$$\frac{\partial \tilde{\rho}_{vA,uB}}{\partial t} = \{i[(\Omega_v - E^{vA}/\hbar) - (\Omega_u - E^{uB}/\hbar)]$$

$$- \gamma_{vA,uB}(1 - \delta_{vu}\delta_{AB})\}\tilde{\rho}_{vA,uB}$$

$$- \frac{i}{2\hbar} \{\mu_{vA,(v+1)C}\tilde{\rho}_{(v+1)C,uB}\mathcal{E}^*$$

$$+ \mu_{vA,(v-1)C}\,\tilde{\rho}_{(v-1)C,uB}\,\mathcal{E}$$

$$- \tilde{\rho}_{vA,(v-1)C}\,\mu_{(v-1)C,uB}\,\mathcal{E}^{*}$$

$$- \tilde{\rho}_{vA,(v+1)C}\,\mu_{(v+1)C,uB}\,\mathcal{E}\ \}$$

$$- \delta_{vu}\delta_{AB}\sum_{qC}\{\tilde{\rho}_{vA,vA}\,w_{vA,qC} - \tilde{\rho}_{qC,qC}\,w_{qC,vA}\} \qquad (52)$$

Only slowly varying quantities appear in (52).

The transformation (47) also enables us to express the slowly varying complex polarization directly in terms of $\tilde{\rho}$:

$$\mathcal{P}(z',t') = 2iN\sum_{A,B}\tilde{\rho}_{vA,(v-1)B}\,\mu_{vA,(v-1)B} \qquad (53)$$

(Eq. (53) follows directly from (46), after some algebra.) Eqs. (52) and (53), together with initial conditions for $\tilde{\rho}$, define the complex polarization which appears in the field propagation equation (44).

Thin-Sample Approximation

The field equation (44) has the formal solution

$$\mathcal{E}(z',t') = [\exp(-\kappa z'/2)]\,\mathcal{E}(0,t')$$

$$+ \frac{k}{2\varepsilon_0}\int_0^{z'}\{\exp[\kappa(z''-z')/2]\}\,\mathcal{P}(z'',t')\,dz'' \,. \qquad (54)$$

$$\equiv \mathcal{E}_{inc}(z',t') + \mathcal{E}_{rad}(z',t') \qquad (55)$$

Physically, the first term in (54) is the incident field, and the second term is the field radiated by the macroscopic polarization $\mathcal{P}$; their sum is the total field $\mathcal{E}$. The spectral content of $\mathcal{E}$ will differ from that of $\mathcal{E}_{inc}$ to the extent that $\mathcal{E}_{rad}$ contains frequencies (or, equivalently, a

time variation) not present in $\mathcal{E}_{inc}$. We shall call the components of $\mathcal{E}_{rad}$ at these new frequencies sidebands.

To facilitate our analytical and numerical studies of the alternation of the spectrum of the field through propagations, we consider the limit in which

$$|\mathcal{E}_{rad}| << |\mathcal{E}_{inc}| , \tag{56}$$

so that we may take[xx]

$$\mathcal{E}(z',t') \cong \mathcal{E}_{inc}(z',t') \tag{57}$$

in calculating the polarization $\mathcal{P}$ by use of (52) and (53). Then (54) implies

$$\mathcal{E}_{rad}(z',t') \cong \frac{k}{2\varepsilon_0} \frac{(1 - e^{-\kappa z'/2})}{\kappa} \mathcal{P}(0,t') \tag{58}$$

If the linear attenuation κ is small (i.e. $\kappa z' << 1$) then

$$\mathcal{E}_{rad}(z',t') \cong \frac{kz'}{2\varepsilon_0} \mathcal{P}(0,t') . \tag{59}$$

Eq. (59) is fundamental for making analytical (and numerical) estimates of the magnitude of the sidebands.

To continue our investigation, and to make the presence of sidebands in $\mathcal{E}_{rad}$ obvious, we make the additional assumption that $\mathcal{E}_{inc}$ is a step pulse:

$$\mathcal{E}_{inc}(0,t') = \begin{cases} 0 & \text{for } t' < 0 \\ E_0 & \text{for } t' > 0 . \end{cases} \tag{60}$$

In what follows we shall also set the linear attenuation κ equal to zero. In view of (60), the coefficients in the density-matrix equation of motion

(52) are independent of time, suggesting an eigenfunction expansion of $\tilde{\rho}$. We shall write (52) in the finite-dimensional matrix form

$$\frac{d\tilde{\rho}}{dt'} = A\tilde{\rho} \tag{61}$$

where we assume the basic $|vA\rangle$ has been truncated to M vectors; we regard $\tilde{\rho}$ as a $(M^2 \times 1)$ column vector, and A as an $(M^2 \times M^2)$ matrix whose components may be read off from (52). Since (61) is linear in $\tilde{\rho}$ and first-order in time, it possesses a solution of the form

$$\tilde{\rho}(t') = V(t',t_0')\ \tilde{\rho}(t_0') \tag{62}$$

where V must satisfy the initial condition

$$V(t_0',t_0') = 1 \ . \tag{63}$$

If we put (62) into (61) and note that $\tilde{\rho}(t_0')$ may be completely arbitrary, we find the following equation for V:

$$\frac{\partial V}{\partial t'} = AV \ . \tag{64}$$

The form of (64) suggests we expand V as

$$V_{v'A',u'B';vA,uB}\ (t',t_0') = \sum_{\lambda} e^{-\lambda(t'-t_0')}\ C_{v'A',u'B'}(\lambda)\ D_{vA,uB}(\lambda) \ . \tag{65}$$

This expansion is in the same spirit as the eigenfunction expansion of $\tilde{\rho}$ used by Goodman and Thiele.[85] The initial condition (63) implies that

$$\sum_{\lambda}\ C_{v'A',u'B'}(\lambda)\ D_{vA,uB}(\lambda) = \delta_{v'v}\delta_{u'u}\delta_{A'A}\delta_{B'B} \ , \tag{66}$$

i.e. that the matrix $D_{vA,uB}(\lambda)$ (with rows ordered by λ and columns by

$(vA,uB))$ is a right inverse of the matrix $C_{v'A',u'B'}(\lambda)$ (with columns ordered by λ and rows ordered by $(v'A',u'B')$). Since a right-inverse matrix is also a left inverse,

$$\sum_{v,u}\sum_{A,B} C_{vA,uB}(\lambda)\, D_{vA,uB}(\lambda') = \delta_{\lambda\lambda'} . \tag{67}$$

Relations (66)-(67) are to be expected for an eigenfunction expansion of the evolution operator v.

We now indicate how the matrix C in (65) may be determined. If we put (65) into (62), we find the following eigenvector-eigenvalue equation:

$$-\lambda C(\lambda) = AC(\lambda) \tag{68}$$

where $C(\lambda)$ is a column vector as noted above.

If we assume the eigenvalue problem (68) has been solved, then the time development of the reduced density matrix $\tilde{\rho}(t')$ (considered as a column vector) is given by (62) and (65):

$$\tilde{\rho}_{vA,uB}(t') = \sum_{\lambda} e^{-\lambda(t'-t_0')} \sum_{v'u'}\sum_{A'B'} C_{vA,uB}(\lambda)\, D_{v'A',u'B'}(\lambda)$$

$$\cdot\, \tilde{\rho}_{v'A',u'B'}(t_0') . \tag{69}$$

From (53) and (69), the slowly varying complex polarization $\mathcal{P}$ is

$$\mathcal{P}(0,t') = \sum_{\lambda} e^{-\lambda(t'-t_0')} \mathcal{P}_{\lambda} \tag{70}$$

where

$$\mathcal{P}_{\lambda} = 2iN \sum_{v,A,B} \mu_{(v-1)A,vB} \sum_{v'u'}\sum_{A'B'} C_{(v-1)A,vB}(\lambda)\, D_{v'A',u'B'}(\lambda)$$

$$\cdot\, \tilde{\rho}_{v'A',u'B'}(t_0') . \tag{71}$$

Equations (70)-(71) are a fundamental result of this paper.

Spectral Content of the Radiated Field

It is evident from (70)-(71) that sidebands will be present in $\mathcal{E}$ whenever the eigenvalues λ have a nonzero imaginary part. We shall now investigate under what physical circumstances this will occur. First, we note that the eigenvalue $\lambda = 0$ corresponds to a steady-state solution of (52) or (61), i.e. a solution in which radiative pumping by the field is exactly balanced by relaxation due to collisions. (In the steady state, $\partial\tilde{\rho}^{ss}/\partial t' = 0$.) Consequently we may identify the eigenvector $C(0)$ corresponding to the zero eigenvalue as the steady-state density matrix (this establishes the normalization of $C(0)$):

$$\tilde{\rho}^{ss} = C(0) \ . \tag{72}$$

It follows from (72), (69) and (67) that if $\tilde{\rho}(t_0') = \tilde{\rho}^{ss}$, then

$$\begin{aligned}\tilde{\rho}_{vA,uB}(t') &= \sum_{\lambda} e^{-\lambda(t'-t_0')} \sum_{v'u'} \sum_{A'B'} C_{vA,uB}(\lambda)\, D_{v'A',u'B'}(\lambda) \\ &\quad \cdot C_{v'A',u'B'}(0) \\ &= \sum_{\lambda} \delta_{\lambda 0}\, e^{-\lambda(t'-t_0')}\, C_{vA,uB}(\lambda) \\ &= \tilde{\rho}^{ss}_{vA,uB}\end{aligned} \tag{73}$$

Eq. (73) expresses the physically reasonable statement that if the system is in the steady state, then it stays in the steady state. Equation (73) also implies, however, that there are no sidebands when the system is in the steady state. It follows that the existence of sidebands is a transient phenomenon, and that the sidebands persist only while the system is evolving toward the steady state.

To calculate the spectral content of the real optical electric field (36), which is expressed in terms of $\mathcal{E}$ as

$$E(z',t') = e\{e^{-i\omega t'}\mathcal{E}(z',t')\}, \tag{74}$$

we calculate the autocorrelation function

$$G(\tau) = \frac{1}{T}\int_0^T [E(z',t'+\tau)\,E(z',t') - E(z',t')^2]dt' \tag{75}$$

which, according to the Wiener-Khinchin theorem, is the Fourier transform of the power spectrum of E. Since the random process represented by E is not stationary, T should not be taken to be longer than the length of the laser pulse. From (74), (70) and (58), we find

$$G(\tau) = \frac{1}{4T}\left[\frac{kz'}{2\varepsilon_0}\right]^2 \{e^{-i\omega\tau}\sum_{\lambda}\sum_{\lambda'}\int_0^T e^{-\lambda^*(t'+\tau)-\lambda' t'}\,\rho_\lambda^*\rho_{\lambda'}\,dt'$$

$$+ \text{complex conjugate}\} \tag{76}$$

where Σ_λ' means a sum on all the eigenvalues

$$\lambda = \lambda_r + i\lambda_i \tag{77}$$

for which $\lambda_i \neq 0$. In (77), λ_r is a relaxation rate, and λ_i is the frequency of the sideband corresponding to the eigenvalue λ. Eq. (76) holds in the limit in which

$$|\lambda_r T| << 1 \tag{78}$$

(i.e., the laser pulse length T is short compared to relaxation times) and

$$|\lambda_i T| >> 1 \tag{79}$$

(i.e., the laser pulse length T is long compared to the period of any of the sideband frequencies). Carrying out the integral in (76), we obtain

$$G(\tau) = \frac{1}{4T}\left[\frac{kz'}{2\varepsilon_0}\right]^2 \sum_{\lambda} \frac{|\mathcal{P}_\lambda|^2}{\lambda+\lambda^*} (1 - e^{-(\lambda+\lambda^*)T}) (e^{(-\lambda^*+i\omega)\tau} + e^{(-\lambda-i\omega)\tau} - 2) \qquad (80)$$

provided we assume that

$$|\lambda_i - \lambda_i'|\, T >> 1 \quad \text{for} \quad \lambda \neq \lambda' \qquad (81)$$

(i.e., the sideband frequencies are all sufficiently different that none of their beat notes are comparable to T^{-1}).

Physically, Eq. (80) says that the intensity of the sideband with frequency $(\omega+\lambda_i)$ is

$$\left[\frac{kz'}{2\varepsilon_0}\right]^2 \frac{1}{4\lambda_r T} (e^{-2\lambda_r T} - 1)\, |\mathcal{P}_\lambda|^2\, e^{-\lambda_r \tau} \qquad (82)$$

This result clearly shows the decay of the sideband intensity to zero for laser pulses which are long compared to the relaxation times of the system. This may be rather simply understood: the system gradually evolves toward the steady state, with time constants which are given by λ_r, according to (69); and in the steady state there are no sidebands.

If the laser pulse is switched on adiabatically starting with $E_0 = 0$, then the system will always be in the steady state corresponding to the present value of E_0. Although the eigenvalues and eigenvectors will also evolve adiabatically, and although there may be some eigenvalues with nonzero imaginary part, there will nevertheless be no observable sidebands because $\mathcal{P}_\lambda$ will vanish for $\lambda \neq 0$.

Generation of Sidebands at Resonant Molecular Transition Frequencies

The sideband frequencies are $(\omega+\lambda_i)$ according to (80). For a qualitative study of λ_i, we turn to simple systems with only a few levels, which are supposed to represent the one $v_3 = 0$ and three $v_3 = 1$ levels shown in Fig. 6. If we label the $v_3 = 0$ level as 0 and the three $v_3 = 1$ levels as 1, 2, and 3 in order of increasing energy, and if we assume the laser frequency ω is such that the $0 \to 1$ transition ($P(J_0)$ in Fig. (6) is resonant, then the detunings $2\Delta_2$ and $2\Delta_3$ of levels 2 and 3 respectively are such that $\Delta_3 > \Delta_2 > 0$ and $\Delta_3 \cong 2\Delta_2$. Further, we shall assume for simplicity that the "typical" transition moments (31) for the $0 \to 1$, $0 \to 2$ and $0 \to 3$ transitions are all equal to μ. We shall also assume that all relaxation rates are negligible

compared to the resonant Rabi frequency (in Hz)

$$\Omega = \frac{\mu E_0}{2h} \quad . \tag{83}$$

The sideband frequencies in the limit

$$\Omega >> \Delta_2 \ , \ \Omega >> \Delta_3 \tag{84}$$

are shown in Table IV, along with the associated polarizations ρ_λ, as determined by an approximate eigenvalue analysis. It will be noticed that the strongest sidebands correspond to $\omega \pm 2\Omega$, and that the next strongest sidebands are at frequencies which (to order Ω) are resonant with the frequencies of the transitions $0 \to 2$ and $0 \to 3$. The electric field strengths at these nearly resonant transition frequencies are

$$\left|\mathcal{E}^{(j)}_{rad}\right| \cong \frac{Nkz'\mu\Omega}{4\varepsilon_0\Delta_j} \tag{85}$$

where $j = 2$ or 3.

If we assume, for example, that $E_0 = 3\times10^7$ V/m (corresponding to an incident intensity of $\sim 1.2\times10^8$ W/cm^2), then $\Omega/c \sim 1$ cm^{-1}. Let us assume $2\Delta_2/c \sim 4$ cm^{-1}, as would be the case for pumping an SF_6 P-branch transition with the P(20) laser line of CO_2 ($\omega/2\pi c \cong 944$ cm^{-1}). We take the transition moment to be $\mu \cong 0.3$ Debye (10^{-30} MKS). We assume a total molecular number density $N \sim 3\times10^{15}$ cm^{-3}, corresponding to a pressure of $\cong 0.1$ torr. We also assume that only those transitions well within a frequency interval Ω of the resonantly pumped line, with roughly $g \cong 10^{-1}$ of the total population, contribute to $\mathcal{E}^{(j)}_{rad}$ at the frequency $\omega+2\Delta_j$, so that the population to be used in (85) is gN rather than N. Then

$$|\mathcal{E}^{(2)}_{rad}| \sim 2\times10^5 \text{ V/m} . \tag{86}$$

We shall give a brief qualitative discussion of the consequences of the phenomenon of resonant sideband generation for multiple-photon excitation in Section V.

Table IV. Approximate Eigenvalues and Associated Polarizations for an Undamped Four-Level System

Sideband frequency $\omega+\lambda_i$	$\mathcal{P}_\lambda$
$\omega \pm 2\Omega$	$\mp iN\mu/2$
$\omega + 2\Delta_2 - \Omega + 0(\Omega^2/\Delta_2)$	$- iN\mu\Omega/2\Delta_2$
$\omega + 2\Delta_3 - \Omega + 0(\Omega^2/\Delta_3)$	$- iN\mu\Omega/2\Delta_3$

Effects of Spatial (M) Degeneracy

The dependence of the transition dipole moment between the effective states $|v\ell JR;M\rangle$ or the molecular eigenstates $\Psi^{v\ell JR}_{pM}$ is given by the 3J symbol in (26). In view of the M selection rule (25), the levels which are radiatively connected to an initial M_0 are not radiatively connected to

a different initial $M_0' \neq M_0$. Let $I = I(v_0 \ell_0 J_0 R_0; M_0)$ be the set of levels which are radiatively connected to the initial state with quantum numbers v_0, ℓ_0, J_0, R_0 and M_0. Then by definition

$$\mu_{vA,uB} = \delta_{I(vA),I(uB)}\, \mu_{vA,uB} , \tag{87}$$

where δ is the Kronecker delta. The sum in (46) then becomes

$$P = N \sum_I \sum_{vA\varepsilon I} \sum_{uB\varepsilon I} \rho_{vA,uB}\, \mu_{vA,uB} . \tag{88}$$

Physically, (88) implies that the total polarization is the sum of the polarizations due to each subset I of radiatively connected states. In view of (69) and the normalization condition

$$\sum_I \sum_{vA\varepsilon I} \rho_{vA,vA} = \sum_I \sum_{vA\varepsilon I} \tilde{\rho}_{vA,vA} = 1 \tag{89}$$

it is convenient to define the population fraction for the Ith subset

$$g_I = \sum_{vA\varepsilon I} \rho_{vA,vA} = \sum_{vA\varepsilon I} \tilde{\rho}_{vA,vA} \tag{90}$$

and the normalized density matrix for the Ith subset

$$\tilde{\rho}^{(I)}_{vA,uB} = (g_I)^{-1}\, \tilde{\rho}_{vA,uB} \qquad (\text{where } vA,uB\varepsilon I) . \tag{91}$$

With these definitions (88) becomes

$$P = N \sum_I g_I \sum_{vA\varepsilon I} \sum_{uB\varepsilon I} \rho^{(I)}_{vA,uB}\, \mu_{vA,uB} , \tag{92}$$

where ρ^I and $\tilde{\rho}^I$ may be calculated as in our previous examples. It may happen, of course, that collisional relaxation couples $\rho^{(I)}$ with $\rho^{(I')}$; for the sake of simplicity we have excluded this possibility in deriving (92), although this is not an essential assumption in our general formalism.

One expects that when all molecules are initially in the vibrational ground state,

$$g_I = \frac{1}{2J_0+1}\, g(J_0) \tag{93}$$

where J_0 is the initial value of J, and $g(J_0)$ is the fraction of molecules with ground-state angular momentum J_0.

Since the transition dipole moment (18) appears to depend strongly on M, and since coherent effects in a resonantly pumped system depend on Rabi frequencies which are directly proportional to the transition dipole moment, it was initially believed that no coherent effects could appear in a system with a large value of J_0. Subsequently, however, it was pointed out by Hopf, Rhodes and Szöke[8] and by Gibbs, McCall and Salamo[9] that the 3J symbol (26), to which the transition dipole moment (18) is proportional, has the property that for certain value of J' and σ many of the values of (26) are very close to one another. This "clustering" of transition moments means that the Rabi frequencies for many M values (for a resonantly pumped two-level system, for example) are very nearly equal, thus enabling the different contributions (I) in (92) to oscillate in phase for a large number of cycles.

The values of the 3J symbol (26) for $J' = J, J+1$, and for $\sigma = 1$ (circularly polarized light) and $\sigma = 0$ (linearly polarized light) are shown in Table V. For $J' = J+1$, $\sigma = 0$, for example, the transition moment is proportional to the function

$$f(M) = [(J+1)^2 - M^2]^{\frac{1}{2}} . \tag{94}$$

It is easy to see that f(M) is a slowly varying function of M near M = 0, so that many of the values of f(M) for M = -J, ..., J are nearly equal to f(0). It should be noted from Table V that the clustering of transition

moments depends on the the change of angular momentum $|J'-J|$ and the polarization σ of the incident field. For P or R branch transitions ($|J'-J| = 1$) the transition moments cluster for linearly polarized light ($\sigma=0$) but not for circularly polarized light ($|\sigma| = 1$). For Q branch transitions ($J'=J$) the reverse is true: the transition moments cluster for circularly polarized light but not for linearly polarized light.

The molecular transition frequencies (shown in the last two lines of Table IV for the example of a four-level system) at which resonant sidebands develop are only weakly affected by the M dependence of the transition moments, while the resonant Rabi frequencies (the first line of Table IV) are strongly affected. Consequently the conclusions drawn above in (85)-(86) are essentially unaltered by the M dependence of the transition moments.

The values of ρ_λ/i summed over initial values of M for a system without damping are shown in Fig. 7. The system employed was our second effective-states model of SF_6 ($|v\ell JR;M\rangle$), with $\sigma = 0$, $J_0 = 68$, $E_0 = 3\times10^5$ V/m, $\omega/2\pi c = 944.2$ cm^{-1}, $\nu_3 = 948$ cm^{-1}, $X_{33} = -2.54$ cm^{-1}, $G_{33} = 0.303$ cm^{-1}, $B = .0907$ cm^{-1}, $\zeta_3 = 0.693$.[xx] The values of ρ_λ/i shown in Fig. 7, obtained by numerical diagonalization followed by summation over all $(2J_0+1) = 137$ values of M_0, clearly show the clustering of resonant Rabi frequencies Ω (84), which directly reflects the clustering of the dipole transition moments (16). Under these conditions E_0 is sufficiently weak that the model SF_6 molecule behaves nearly as a two-level system, as far as the sidebands in the first line of Table IV are concerned.

The values of ρ_λ/i summed over initial values of J_0 and M_0, under conditions of stronger radiative driving ($E_0 = 3\times10^7$ V/m), are shown in Fig. 8. The sidebands at small detuning correspond roughly to the first

line of Table IV; the sidebands at larger detunings are approximately at resonant molecular transition frequencies. The calculations which resulted in Fig. 8 involved a summation over 49 values of J_0 and 11 values of M_0 for each J_0.

Table III. Spectroscopic Parameters for the ν_3 Fundamental of SF_6^{13}

Parameter (see Table II)	Value (cm^{-1}) and Standard Deviation
m	947.9763307(62)
n	$5.581731(39) \times 10^{-2}$
p	$-1.615414(89) \times 10^{-4}$
q	$1.236(47) \times 10^{-8}$
s	$-6.77(23) \cdot 10^{-11}$
t	$-5.8(9.0) \times 10^{-14}$
v	$-6.9876(46) \cdot 10^{-5}$
w	$-0.9(1.3) \times 10^{-11}$
g	$-2.45621(32) \quad 10^{-5}$
h	$-1.910(12) \times 10^{-9}$
k	$-1.54(11) \times 10^{-11}$
u	$0.4(1.0) \times 10^{-11}$

Table V. Values of the 3J Symbol[62]

J'	σ	$\begin{pmatrix} J & 1 & J' \\ M & \sigma & -(M+\sigma) \end{pmatrix}$
J	1	$(-1)^{J-M-1}\left[\frac{(J-M)(J+M+1)}{2J(J+1)(2J+1)}\right]^{\frac{1}{2}}$
J	0	$(-1)^{J-M-1}\frac{M}{[J(J+1)(2J+1)]^{\frac{1}{2}}}$
$J+1$	1	$(-1)^{J-M-1}\left[\frac{(J+M+1)(J+M+2)}{(2J+1)(2J+2)(2J+3)}\right]^{\frac{1}{2}}$
$J+1$	0	$(-1)^{J-M}\left[\frac{(J-M+1)(J+M+1)}{(J+1)(2J+1)(2J+3)}\right]^{\frac{1}{2}}$

V. SUMMARY AND DISCUSSION

We have established the following points with regard to the optical field radiated by the macroscopic polarization which is set up in a molecular gas irradiated by a pulsed laser field:

(i) The sideband field is proportional to $\mu N k z'$ and the sideband intensity is proportional to $(\mu N k z')^2$, in the limit where the radiated field is small compared to the incident field, and where no significant reabsorption of the radiated field occurs.

(ii) The sideband intensity approaches zero as the molecules approach equilibrium between radiative pumping and collisional (or intramolecular) relaxation. Sidebands will be observable only if the risetime of the laser pulse is short compared to the shortest collisional (or intramolecular) relaxation time.

(iii) Sidebands are generated in near resonance with every molecular transition accessible from the initial state of the molecules.

The most qualitatively important effect from the point of view of multiple-photon excitation of polyatomic molecules is (iii), since this result implies that a laser pulse generates essentially every transition frequency of the molecular vibration-rotation band with which it interacts, as a result of the process of propagation. In particular, this collective generation of new frequencies is the only process known to us which can explain the very large number of rotational states in SF_6 pumped by a CO_2 laser at rather modest laser intensities.[30] To illustrate this point, let us consider the Rabi frequency at which molecules will cycle population between levels 0 and 2 as a result of the coherently generated field (86). The Rabi frequency for population cycling is

$$\frac{\mu|\mathcal{E}^{(2)}_{rad}|}{h} \sim 3\times10^{8}\ s^{-1} \qquad (95)$$

i.e. the Rabi period is ~ 3 ns, under the conditions assumed for (86). Averaged over in times long compared to 3 ns, then, half the molecular population in state 0 will appear in state 2, under the influence of the field $\mathcal{E}^{(2)}_{rad}$. This time for nearly saturated pumping of level 2 is less than the 50-100 ns CO_2 laser pulse lengths often employed in experiments on multiple-photon excitation of SF_6. The predicted time-averaged probability of 0.5 for excitation of level 2 by the field $\mathcal{E}^{(2)}_{rad}$ in this case should be contrasted with the time-averaged probability of excitation of level 2 produced by the incident field $\mathcal{E}_{inc}$ acting alone, which is

$$\left[\frac{\Omega}{2\Delta_2}\right]^2 \sim 6\times10^{-2}\ . \qquad (96)$$

For weaker incident fields, $(\Omega/2\Delta_2)^2$ is smaller (in proportion to the incident intensity), and the enhancement of excitation by $\mathcal{E}^{(2)}_{rad}$ (for sufficiently long laser pulses and low relaxation rates) is even greater than in this example.

Although the estimates just presented depend on the assumption of no collisional or unimolecular relaxation during the time of the laser pulse (according to (ii)), this assumption should be fulfilled for collisional effects at the pressure (~ 0.1 torr) assumed in deriving (86), for laser pulses of length T < 100 ns. In applying result (ii), it should also be noted that any major change in laser pulse amplitude or frequency will have the effect of disequilibrating the molecular populations and enabling a renewed generation of sidebands. Even unstabilized CW lasers may be able to generate sidebands in SF_6 and other molecular gases, due to

frequency jitter and a consequent lack of equilibrium between laser pumping and collisional relaxation.

The conditions for efficient experimental observation of sidebands are evidently

$$T \ll \text{shortest relaxation time} \tag{97}$$

$$T \ll |h/\mu \mathcal{E}_{rad}^{(j)}| \tag{98}$$

$$T \gg (2\Delta_j)^{-1} \tag{99}$$

where T is the laser pulse length. Condition (97) is required by (ii). Condition (98) means physically that the radiated field does not strongly excite any molecules, and thus is able to escape from the sample cell. Condition (99), which will be fulfilled in practice for all but the shortest pulses, simply means that the sidebands can execute many periods of oscillation with respect to the incident frequency, so that there is a well-defined frequency for either spectral or temporal observation.

The functional dependence of sideband-induced effects on the product $\mu N k z'$ as stated in (i) provides a way to distinguish the effects of collective, coherent generation of sidebands from unimolecular or collisional relaxation. For unimolecular relaxation there should be no dependence on N or z'. For collisional relaxation, the increase of energy absorbed per molecule due to collisions might be expected to be proportional to N. In certain limits the molecular excitation produced by (for example) $\mathcal{E}_{rad}^{(2)}$ (85) will be roughly proportional to N, for fixed z'; this dependence could easily be mistaken for a collisional effect. True collisional effects can, in principle, be distinguished from coherent propagation effects under the conditions (97)-(99) by a study of the dependence on z', for a fixed N.

In view of (ii), the experimental observation of sidebands in SF_6 (or other polyatomic molecules) would be evidence that the collisional or intramolecular relaxation time is not much shorter in order to magnitude than the laser pulse length T. Clearly, if (for example) SF_6 relaxes to thermodynamic equilibrium with resonant laser light in a very short time, as some have claimed,[21] then no sidebands should be observed according to (73). Experiments to observe sideband production may, in fact, provide a way to distinguish unambiguously between coherent excitation (which produces sidebands) and unselective laser heating of the molecules (which produces no sidebands). Quantitative measurements of the energy transferred to sidebands, and comparison with theoretical results such as (80), may be a useful technique for measuring (or for putting a lower limit on intramolecular relaxation times.

Sidebands may, in principle, be observed either spectroscopically or temporally. Temporal observation (i.e., observation of optical nutation) depends on the fact that the intensity of the total field, which is proportional to

$$|\mathcal{E}(z',t')|^2 = |\mathcal{E}_{inc}(t')|^2 + 2\mathrm{Re}(\mathcal{E}_{inc}(t')\,\mathcal{E}_{rad}(z',t')^*) + |\mathcal{E}_{rad}(t')|^2 \qquad (100)$$

The advantage of temporal observation is that the heterodyne term $2\mathrm{Re}(\mathcal{E}_{inc}\mathcal{E}^*_{rad})$ in (100), which will display temporal oscillations at the dominant sideband frequency (Fig. 9), provides a substantial amplification of the weak field $\mathcal{E}_{rad}$. The disadvantage of temporal observation is that the presence of many different sideband frequencies leads gradually to destructive interference, causing the oscillations to decay in amplitude.

Such a decay is a well-known consequence of the range of Rabi frequencies induced by Doppler broadening.[6] Similar phenomena in optical free induction decay have recently discussed theoretically in the context of electronic molecular transitions.[86] The advantage of spectroscopic observation is, of course, that the sidebands may be observed even if the range of sideband frequencies is so great that only a very few temporal oscillations appear. The disadvantage is that the sideband intensity may be very weak, except for the relatively strong sidebands at the resonant Rabi frequency (see the first line of Table IV).

A number of points which we have not addressed in this work deserve further study, and will be subjects of our continuing research. First, we have not given any quantitative treatment of the effects of sideband generation on the energy deposited in a molecular gas by an incident laser pulse. This promises to be a challenging problem in radiative transport. Second, we have considered no coherent propagation effects other than sideband generation.[87] In particular, we have not yet addressed the question of explaining the photon-echo data in SF_6.[28] Although we have made numerical studies of optical free induction decay, space has not permitted us to discuss them here. Finally, we have not discussed effects due to the transverse variation of the incident field.

We believe that our calculations reported in this paper have established that the consequences of sideband generation for multiple-photon excitation of polyatomic molecules deserve serious study. We expect to report our continuing studies of this problem in future publications.

VI. ACKNOWLEDGEMENTS

We thank R. V. Ambartzuman, K. Boyer, C. B. Collins, B. J. Feldman, R. A. Fisher, D. Ham, J. Jortner, O. P. Judd and V. S. Letokhov for helpful discussions.

Figure Captions

Fig. 1. Atomic displacments in one of the ν_3 and one of the ν_4 modes of SF_6, as determined from the force-field analysis of McDowell et al.[31] (Figure courtesy of R. S. McDowell).

Fig. 2. The absorption spectrum of the ν_3 band of SF_6 at a temperature T = 153K. (Courtesy of K. N. Rao, S Hurlock, P. L. Houston and J. J. Steinfeld.[41]) The P, Q, and R branches are clearly evident, but no rotational structure is visible.

Fig. 3. The absorption spectrum of the central portion of the ν_3 band of SF_6 near 948 cm^{-1} at a temperature of 135K, obtained with a semiconductor diode laser.[47] The center trace shows the Q branch.

Fig. 4. The absorption spectrum of room-temperature SF_6 near the P(16) CO_2 laser line at 947.7417 cm^{-1}, obtained with a semiconductor diode laser and calibrated by heterodyning with a stable CO_2 laser operating on the P(16) line.[11] SF_6 spectroscopic assignments are indicated. Total tuning range approximately ±1 GHz.

Fig. 5. The saturation spectrum of room-temperature SF_6 near the P(16) CO_2 laser line at 947.7417363 cm^{-1}, calibrated by offset frequency locking to a stable CO_2 laser locked on an SF_6 absorption line.[13] Total tuning range approximately - 250 MHz to + 250 MHz.

Fig. 6. States in SF_6 radiatively connected to one value of $J(=J_0)$ in the vibrational ground state. For clarity only ν_3 = 0, 1, and 2 are shown.

Fig. 7. Sideband amplitudes ($_\lambda$/i) summed over all initial M values for a single ground-state angular momentum J_0 = 68, plotted as a

function of detuning (λ_i). All relaxation rates were zero in this calculation. Other parameters are given in the text.

Fig. 8. Sideband amplitudes (λ/i) averaged over 11 initial M values from M = -J to +J and over 49 initial J values from J_0 = 5 to 101, plotted as a function of detuning (λ_i). All relaxation rates were zero in this calculation. Other parameters are given in the text. Total frequency range: -6.91 to +6.91 cm^{-1}. The peak at +4 on the horizontal scale is a sideband in resonance with the Q branch. The peak at +7 is in resonance with R-branch transitions originating near J_0 = 68.

Fig. 9. Amplitude | | and phase ϕ of the total field (55) at z' = 10 cm as a function of retarded time t'. Conditions same as for Fig. 8. Total time interval: 0 to 48.3 ps.

References

1. C. K. N. Patel and R. E. Slusher, Phys. Rev. Lett. 19, 1019 (1967).

2. C. K. N. Patel and R. E. Slusher, Phys. Rev. Lett. 20, 1087 (1968).

3. G. B. Hocker and C. L. Tang, Phys. Rev. 184, 356 (1969).

4. A. Zembrod and Th. Grühl, Phys. Rev. Lett. 27, 287 (1971).

5. S. S. Alimpiev and N. V. Karlov, Sov. Phys.-JETP 39, 260 (1974).

6. C. L. Tang and B. D. Silverman, pp. 280-293 in Physics of Quantum Electronics, ed. by P. L. Kelly, B. Lax and P. E. Tannenwald (McGraw-Hill, New York, 1966).

7. F. A. Hopf and M. O. Scully, Phys. Rev. B 1, 50 (1970).

8. F. A. Hopf, C. K. Rhodes and A. Szöke, Phys. Rev. B 1, 2833 (1970).

9. H. M. Gibbs, S. L. McCall and G. J. Salamo, Phys. Rev. A 12, 1032 (1975).

10. R. S. McDowell, H. W. Galbraith, B. J. Krohn, C. D. Cantrell, and E. D. Hinkley, Optics Commun. 17, 178 (1976).

11. R. S. McDowell, H. W. Galbraith, C. D. Cantrell, N. G. Nereson and E. D. Hinkley, J. Mol. Spectrosc. 68, 288 (1977).

12. R. S. McDowell, H. W. Galbraith, C. D. Cantrell, N. G. Nereson, P. F. Moulton and E. D. Hinkley, Optics Lett. 2, 97 (1978).

13. Ch. J. Bordé, M. Ouhayonn, A. VanLerberghe, C. Salomon, S. Avrillier, C. D. Cantrell, and J. Bordé, Proceedings of the Fourth International Conference on Laser Spectroscopy, ed. by H. Walther (in press).

14. C. D. Cantrell and H. W. Galbraith, Optics Commun. 18, 513 (1976); 21, 374 (1977).

15. V. M. Akulin, S. S. Alimpiev, N. V. Karlov, B. G. Sartakov, and L. A. Shelepin, ZhETF 71, 454 (1976).

16. C. D. Cantrell, H. W. Galbraith and J. R. Ackerhalt, pp. 307-330 in Multiphoton Processes, ed. by J. H. Eberly and P. Lambropoulos (Wiley, New York, 1978).

17. H. W. Galbraith and C. D. Cantrell, pp. 227-264 in The Significance of Nonlinearity in the Natural Sciences, ed. by B. Kursunoglu, A. Perlmutter and L. F. Scott (Plenum, New York, 1977).

18. C. D. Cantrell and K. Fox, Optics Lett. 2, 151 (1978).

19. J. R. Ackerhalt and H. W. Galbraith, J. Chem. Phys. 69, 1200 (1978).

20. P. F. Moulton and A. Mooradian, pp. 37-42 in Laser-Induced Processes in Molecules, ed. by K. L. Kompa and S. D. Smith (Springer, Berlin, 1979).

21. H. S. Kwok and E. Yablonovitch, Phys. Rev. Lett. 41, 745 (1978).

22. W. E. Lamb, Jr., Phys. Rev. 134, A1429 (1964).

23. F. A. Hopf and M. O. Scully, Phys. Rev. 179, 399 (1969).

24. A. Icsevgi and W. E. Lamb, Jr., Phys. Rev. 185, 517 (1969).

25. C. D. Cantrell and W. H. Louisell (to be published).

26. R. L. Shoemaker, pp. 453-504 in Laser Applications to Optics and Spectroscopy, ed. by S. F. Jacobs, M. Sargent III, J. F. Scott and M. O. Scully (Addison-Wesley, Reading, Mass., 1975).

27. N. A. Kurnit, I. D. Abella and S. R. Hartmann, Phys. Rev. Lett. 13, 567 (1964); Phys. Rev. 141, 391 (1964).

28. C. V. Heer and R. J. Nordstrom, Phys. Rev. A 11, 536 (1975); W. M. Gutman and C. V. Heer, Phys. Rev. A 16, 659 (1977).

29. A. A. Makarov, C. D. Cantrell and W. H. Louisell, Optics Commun. (to be published).

30. S. S. Alimpiev, V. N. Bagratashvili, N. V. Karlov, V. S. Letokhov, V. V. Lobko, A. A. Makarov, B. G. Sartakov, and E. M. Khokhlov, ZhETF Pis. Red. 25, 582 (1977); A. S. Akhmanov, V. N. Bagratashvili, V. Yu. Baranov, Yu. R. Kolomisky, V. S. Letokhov, V. D. Pismenny and E. A. Ryabov, Optics Commun. 23, 357 (1977).

31. R. S. McDowell, J. P. Aldridge and R. F. Holland, J. Phys. Chem. 80, 1203 (1976).

32. B. T. Darling and D. M. Dennison, Phys. Rev. 57, 128 (1940).

33. J. K. G. Watson, Mol. Phys. 15, 479 (1968).

34. J. D. Louck, J. Mol. Spectrosc. 61, 107 (1976).

35. Yu. S. Makushkin and O. N. Ulenikov, J. Mol. Spectrosc. 68, 1 (1977).

36. W. H. Shaffer, H. H. Nielsen and L. H. Thomas, Phys. Rev. 56, 895 and 1051 (1939).

37. J. Moret-Bailly, J. Mol. Spectrosc. 15, 344 (1965).

38. K. T. Hecht, J. Mol. Spectrosc. 5, 355 (1960).

39. K. Fox, B. J. Krohn and W. H. Shaffer, J. Chem. Phys. (to be published).

40. H. Brunet and M. Perez, J. Mol. Spectrosc. 29, 472 (1969); H. Brunet, IEEE J. Quant. Elect. QE-6, 678 (1970).

41. P. L. Houston and J. I. Steinfeld, J. Mol. Spectrosc. 54, 335 (1975); K. N. Rao and S. Hurlock, private communication.

42. E. D. Hinkley, Appl. Phys. Lett. 13, 49 (1968).

43. E. D. Hinkley and P. L. Kelley, Science 171, 635 (1971).

44. K. W. Nill, F. A. Blum, A. R. Calawa and T. C. Harman, Appl. Phys. Lett. 19, 79 (1971).

45. E. D. Hinkley, Appl. Phys. Lett. 16, 351 (1970).

46. R. S. McDowell, in Advances in Infrared and Raman Spectroscopy, ed. by R. J. H. Clark and R. E. Hester (Heyden & Son, London, 1977).

47. J. P. Aldridge, H. Filip, H. Flicker, R. F. Holland, R. S. McDowell, N. G. Nereson and K. Fox, J. Mol. Spectrosc. 58, 165 (1975).

48. C. D. Cantrell, Los Alamos Scientific Laboratory Informal Report LA-5464-MS (1973).

49. C. D. Cantrell and H. W. Galbraith, J. Mol. Spectrosc. 58, 158 (1975).

50. K. Fox and W. B. Person, J. Chem. Phys. 64, 5218 (1976).

51. K. Fox, Optics Commun. 19, 397 (1976).

52. S. L. McCall and E. L. Hahn, Phys. Rev. 183, 457 (1969).

53. I. Burak, A. V. Nowak, J. I. Steinfeld and D. G. Sutton, J. Chem. Phys. 51, 2275 (1969).

54. J. I. Steinfeld, I. Burak, D. G. Sutton and A. V. Nowak, J. Chem. Phys. 52, 5421 (1970).

55. D. S. Frankel and J. I. Steinfeld, J. Chem. Phys. 62, 3358 (1975).

56. A. V. Nowak and J. L. Lyman, J. Quant. Spectrosc. Radiat. Transf. 15, 945 (1975).

57. P. F. Moulton, D. M. Larsen, J. N. Walpole and A. Mooradian, Optics Lett. 1, 51 (1977).

58. J. Moret-Bailly, L. Gautier and J. Montagutelli, J. Mol. Spectrosc. 15, 355 (1965).

59. H. H. Nielsen, pp. 173-313 in Encyclopedia of Physics, Vol. 37/1, ed. by S. Flügge (Springer, Berlin, 1959).

60. M. Abramowitz and I. A. Stegun, Handbook of Mathematical Functions, (U.S. Government Printing Office, Washington, 1964).

61. E. P. Wigner, Group Theory and Its Application to the Quantum Mechanics of Atomic Structure, tr. by J. J. Griffin (Academic Press, New York, 1959), Ch. 19.

62. D. M. Brink and G. R. Satchler, Angular Momentum, 2nd edition (Clarendon Press, Oxford, 1971).

63. K. Fox and B. J. Krohn, J. Comp. Phys. 25, 386 (1977).

64. B. J. Krohn, private communication.

65. J. Moret-Bailly, Cah. Phys. 15, 237 (1961).

66. J. D. Louck, Ph.D. thesis (unpublished).

67. A. G. Robiette, D. L. Gray and F. W. Birss, Mol. Phys. 32, 1591 (1976).

68. B. Bobin and K. Fox, J. Phys. (Paris) 34, 571 (1973).

69. C. D. Cantrell, S. Avillier, Ch. Salomon and Ch. J. Bordé (to be published).

70. F. R. Petersen, D. G. McDonald, J. D. Cupp and B.L. Danielson, p. 555 in Laser Spectroscopy, ed. by R. G. Brewer and A. Mooradian (Plenum, New York, 1974).

71. J. L. Hall, IEEE J. Quant. Elect. QE-4, 638 (1968); R. L. Barger and J. L. Hall, Phys. Rev. Lett. 22, 4 (1969).

72. K. Fox, Optics Lett. 1, 214 (1977).

73. H. W. Galbraith, Optics Lett. 3, 154 (1978).

74. C. D. Cantrell (unpublished).

75. J. S. Briggs (unpublished).

76. I. N. Knyazev, V. S. Letokhov and V. V. Lobko, Optics Commun. 25, 337 (1978).

77. D. M. Larsen and N. Bloembergen, Optics Commun. 17, 254 (1976).

78. D. M. Larsen, Optics Commun. 19, 404 (1976).

79. C. J. Elliott and B. J. Feldman, Bull. Am. Phys. Soc. 20, 1282 (1975).

80. S. Mukamel and J. Jortner, Chem. Phys. Lett. 40, 150 (1976).

81. R. V. Ambartzumian, Yu. A. Gorokhov, V. S. Letokhov, G. N. Makarov and A. A. Puretzky, ZhETF Pis. Red. 23, 26 (1976) [JETP Lett. 23, 22 (1976)].

82. C. D. Cantrell, W. H. Louisell and J. F. Lam, pp. 138-141 in Laser-Induced Processes in Molecules, ed. by K. L. Kompa and S. D. Smith (Springer, Berlin, 1979).

83. J. Stone, M. F. Goodman and D. A. Dows, J. Chem. Phys. 65, 5062 (1976).

84. C. D. Cantrell, S. M. Freund and J. L. Lyman, in Laser Handbook, Vol. III(b), ed. by M. L. Stitch (North-Holland, Amsterdam, 1979).

85. M. F. Goodman and E. Thiele, Phys. Rev. A 5, 1355 (1972).

86. J. Jortner and J. Kommandeur, Chem. Phys. 28, 273 (1978).

87. O. P. Judd (to be published).

CARTESIAN DISPLACEMENT COORDINATES
FOR THE INFRARED-ACTIVE
FUNDAMENTAL VIBRATIONS OF SF_6

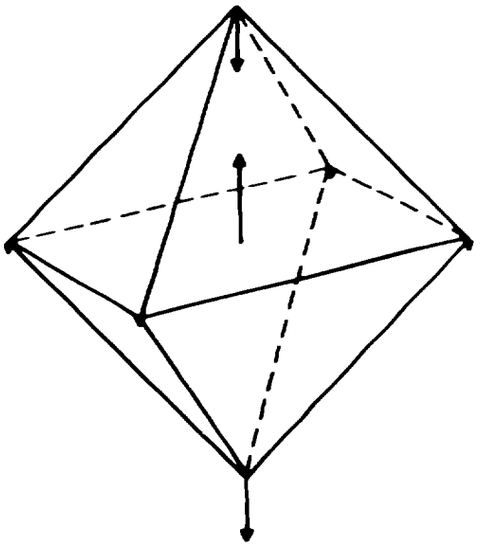

ν_3 MODE

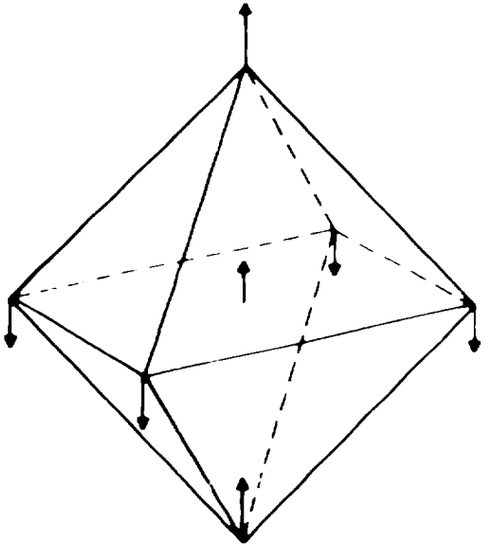

ν_4 MODE

Fig. 1

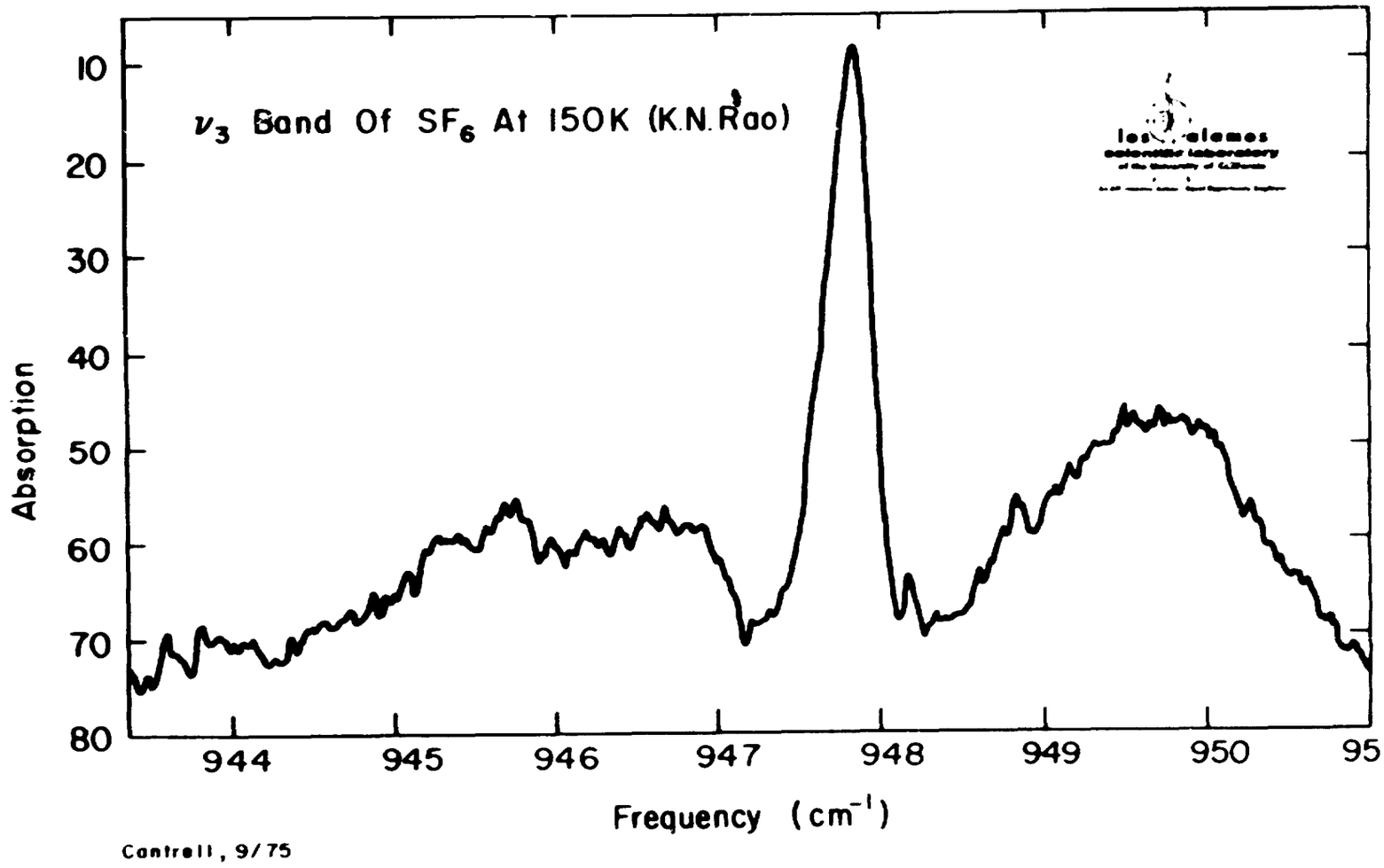
ν_3 Band Of SF_6 At 150K (K.N.Rao)
los alamos
scientific laboratory
Absorption
10
20
30
40
50
60
70
80
944
945
946
947
948
949
950
951
Frequency (cm^{-1})
Cantrell, 9/75

Fig. 2

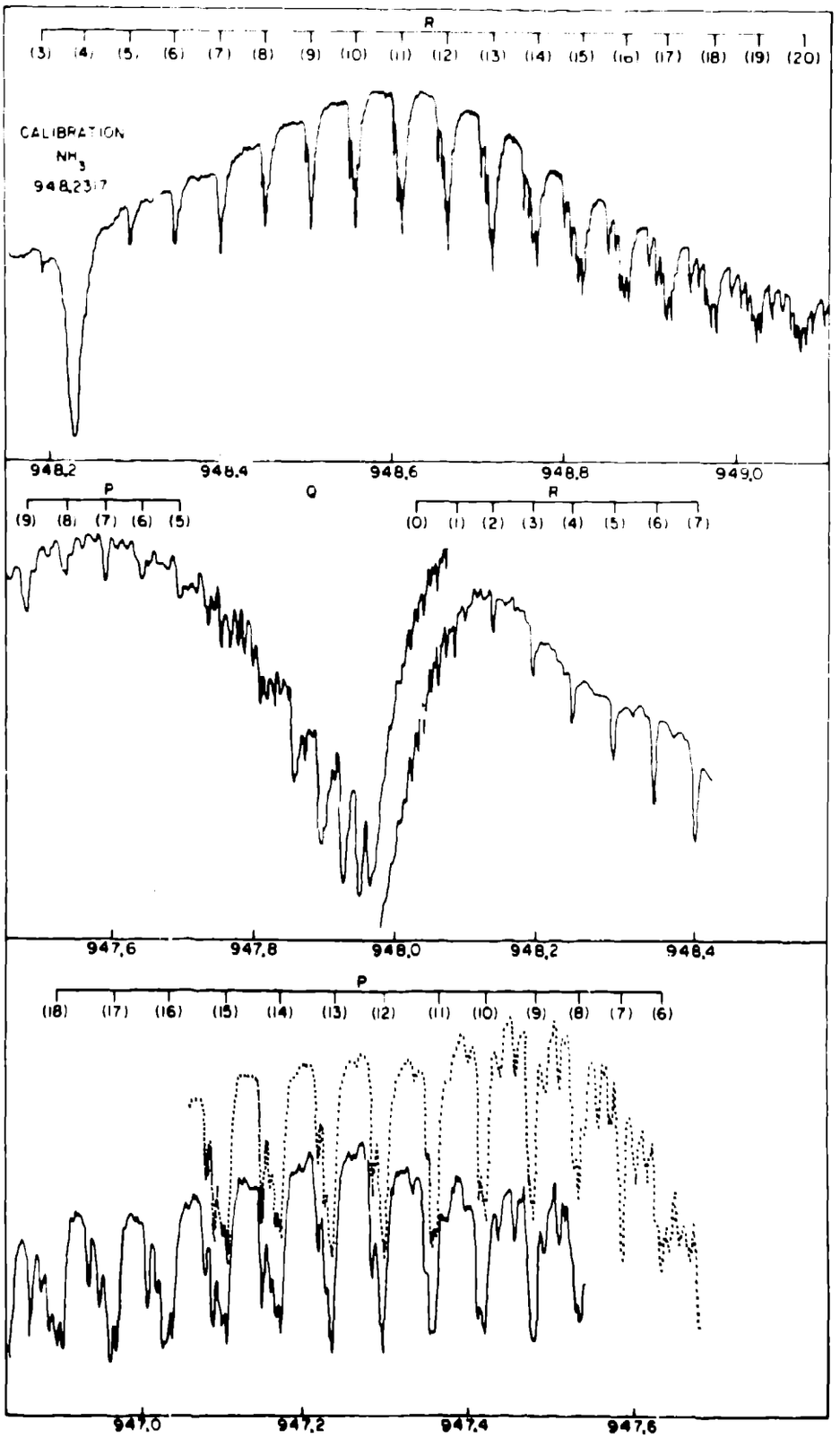
R
(3) (4) (5) (6) (7) (8) (9) (10) (11) (12) (13) (14) (15) (16) (17) (18) (19) (20)
CALIBRATION
NH3
948,23
948.2
948.4
948.6
948.8
949.0
P
(9) (8) (7) (6) (5)
Q
R
(0) (1) (2) (3) (4) (5) (6) (7)
947.6
947.8
948.0
948.2
948.4
P
(18) (17) (16) (15) (14) (13) (12) (11) (10) (9) (8) (7) (6)
947.0
947.2
947.4
947.6

Fig. 3

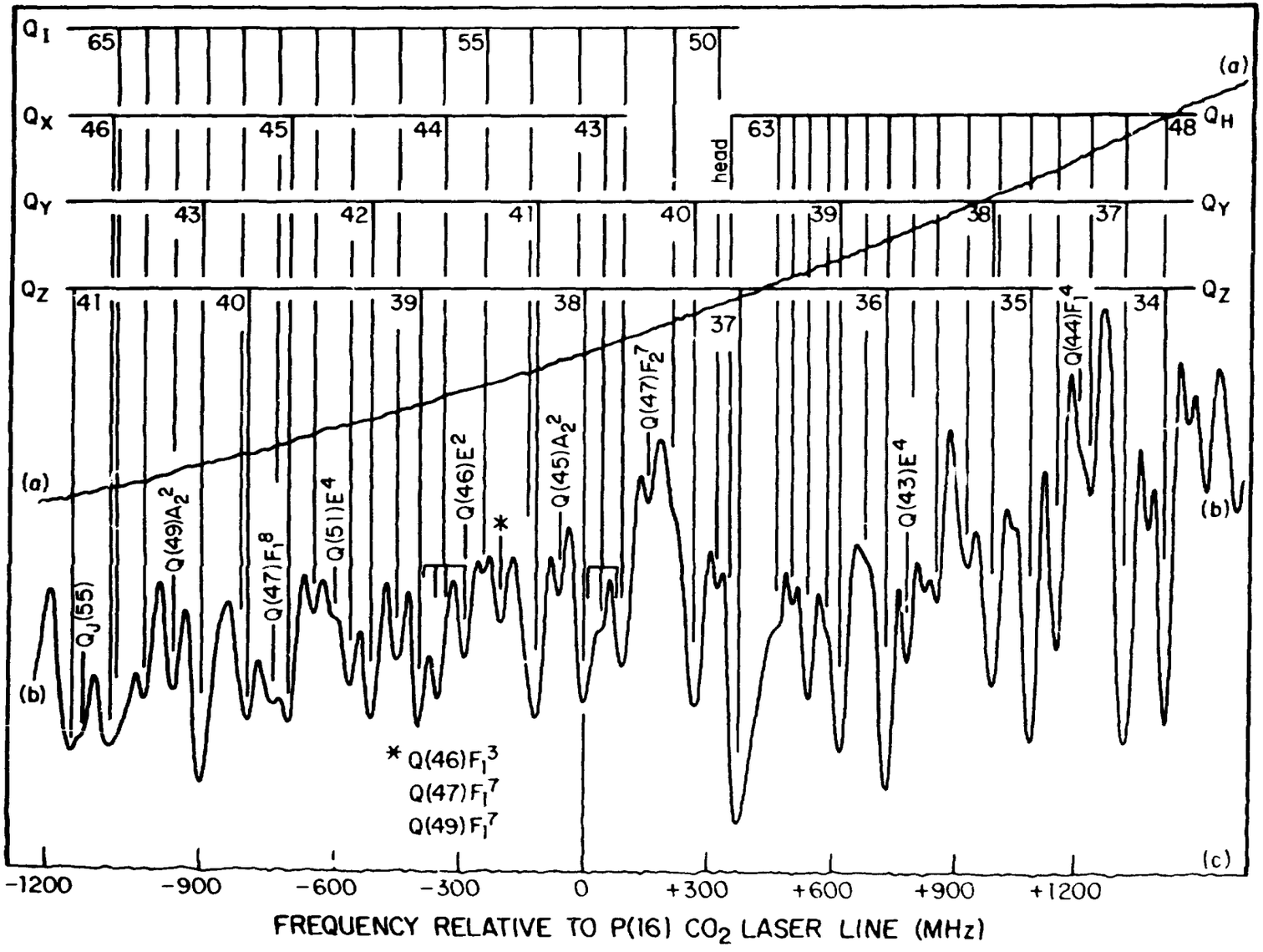
Q_I
65
55
50
Q_X
46
45
44
43
head
63
48
Q_H
Q_Y
43
42
41
40
39
38
37
Q_Z
41
40
39
38
37
36
35
34
(a)
(b)
(c)
$Q_J(55)$
$Q(49)A_2^2$
$Q(47)F_1^8$
$Q(51)E^4$
$Q(46)E^2$
*
$Q(45)A_2^2$
$Q(47)F_2^7$
$Q(43)E^4$
$Q(44)F_1^4$
* $Q(46)F_1^3$
$Q(47)F_1^7$
$Q(49)F_1^7$
-1200
-900
-600
-300
0
+300
+600
+900
+1200
FREQUENCY RELATIVE TO P(16) CO_2 LASER LINE (MHz)

Fig. 4

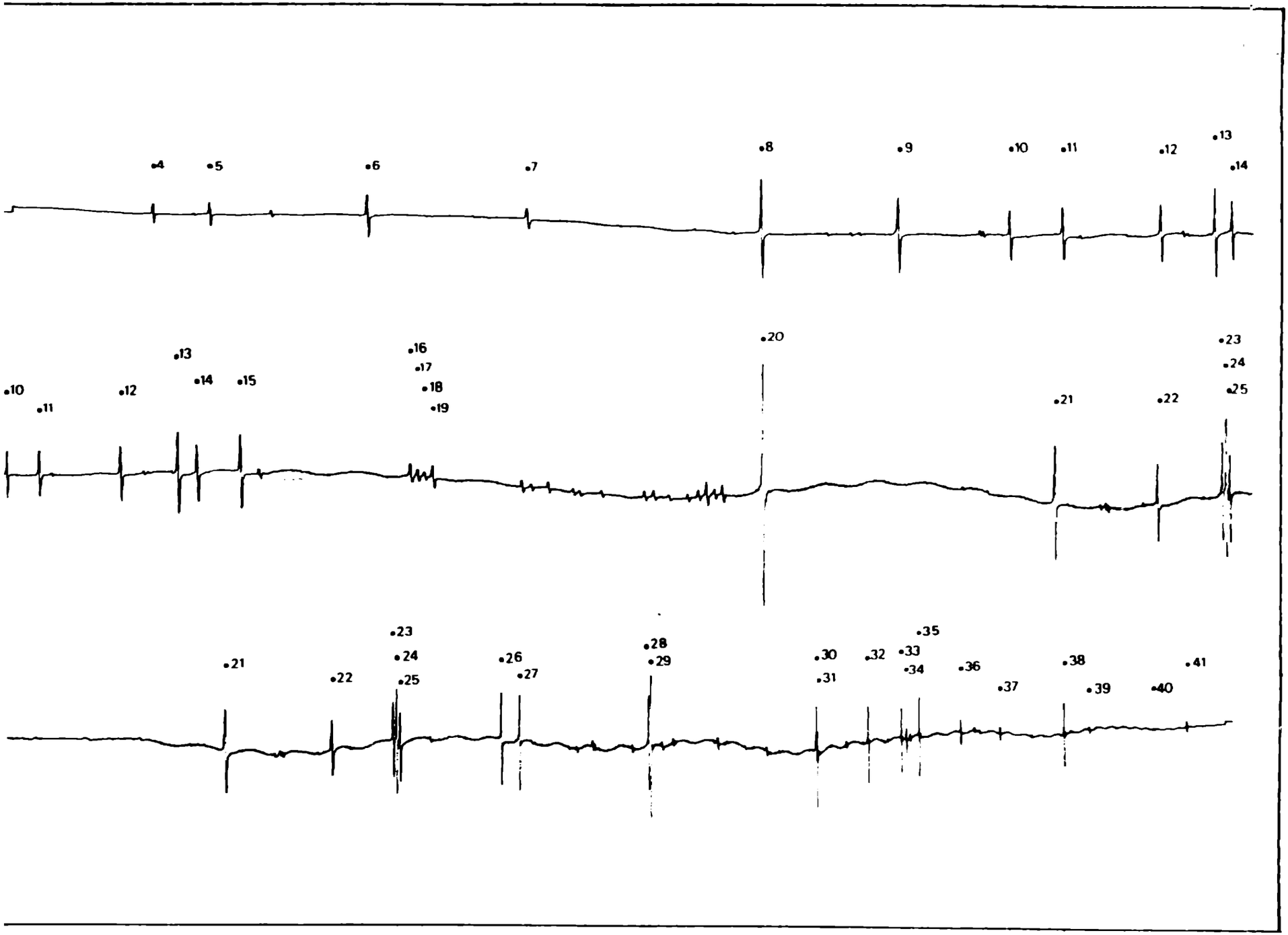
•4
•5
•6
•7
•8
•9
•10
•11
•12
•13
•14
•10
•11
•12
•13
•14
•15
•16
•17
•18
•19
•20
•21
•22
•23
•24
•25
•21
•22
•23
•24
•25
•26
•27
•28
•29
•30
•31
•32
•33
•34
•35
•36
•37
•38
•39
•40
•41

Fig. 5

los alamos
scientific laboratory
of the University of California

RADIATIVELY CONNECTED STATES IN SF_6
(WITH A CONSTANT VALUE OF ROTATIONAL ANGULAR MOMENTUM R)

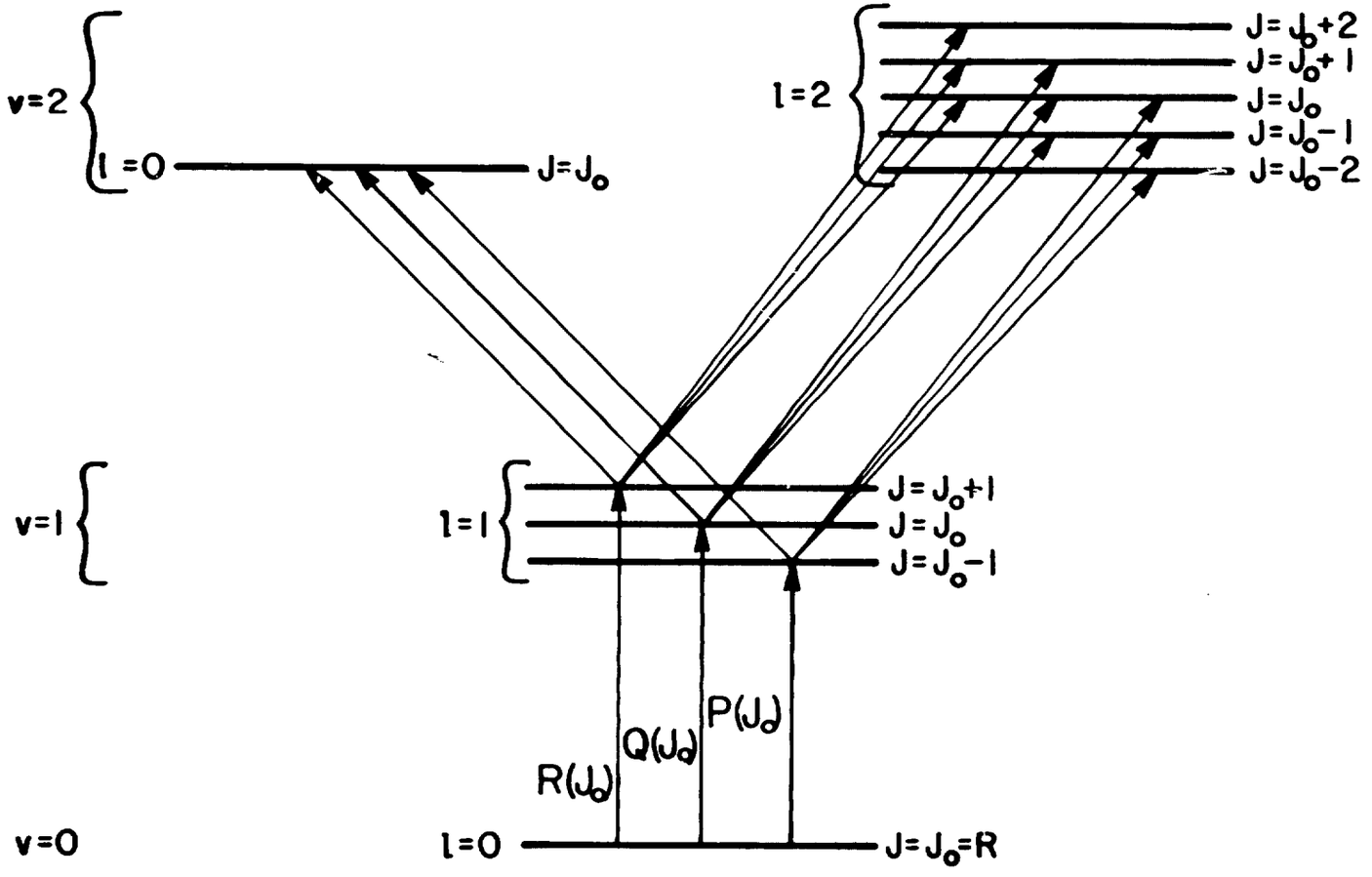

Fig. 6

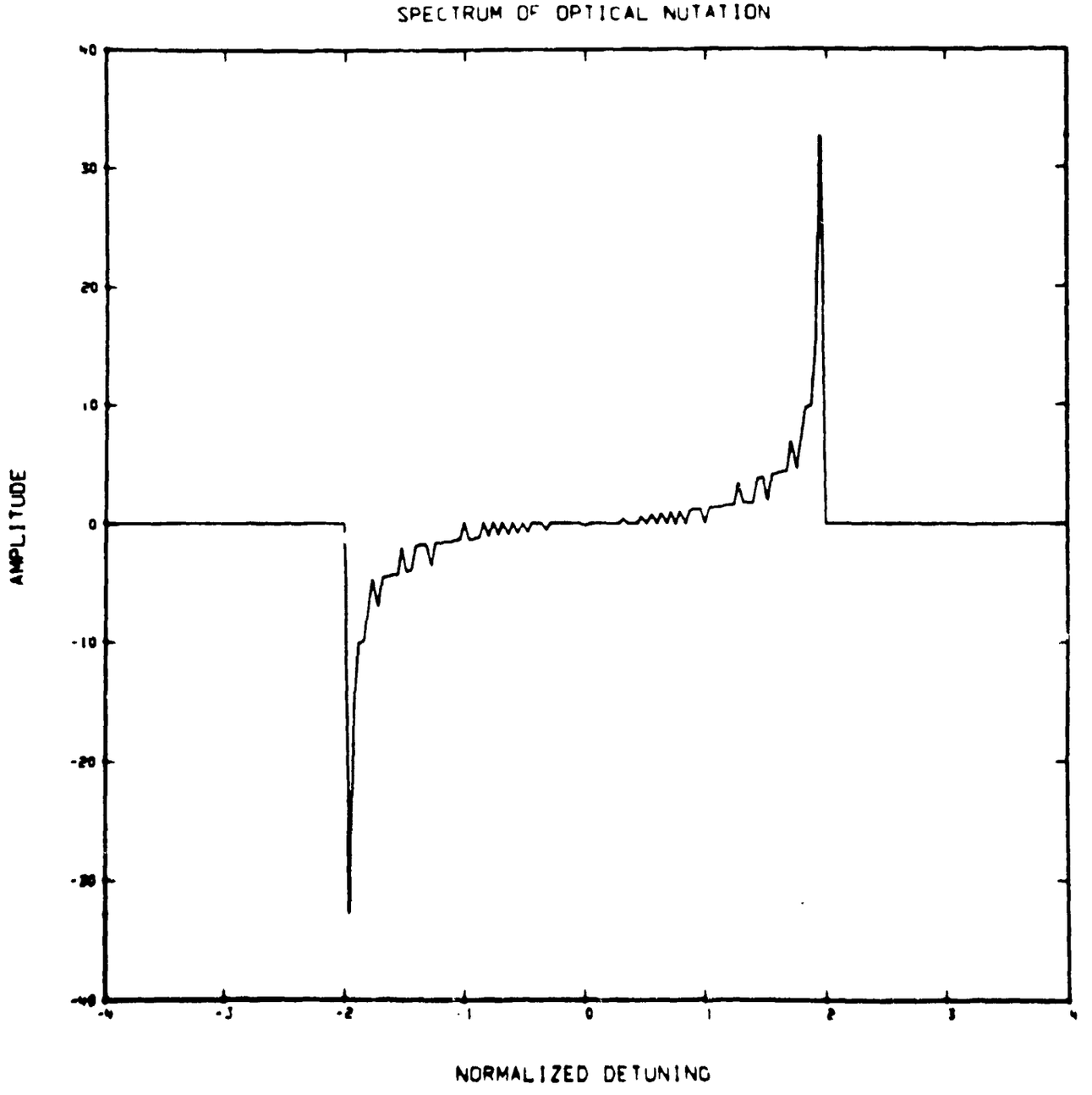
SPECTRUM OF OPTICAL NUTATION
AMPLITUDE
NORMALIZED DETUNING
40
30
20
10
0
-10
-20
-30
-40
-4
-3
-2
-1
0
1
2
3
4

Fig. 7

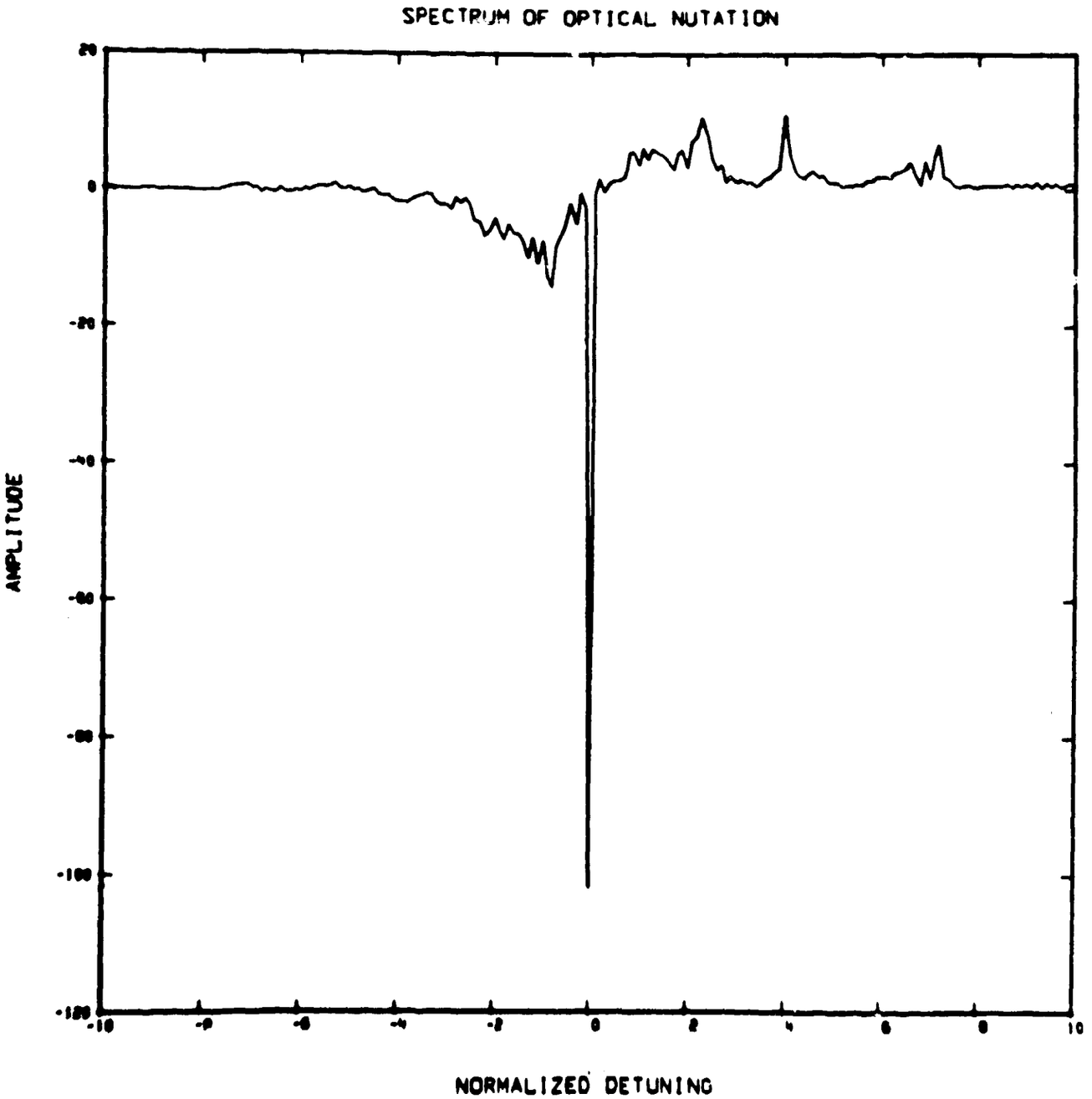
SPECTRUM OF OPTICAL NUTATION
AMPLITUDE
NORMALIZED DETUNING

Fig. 8

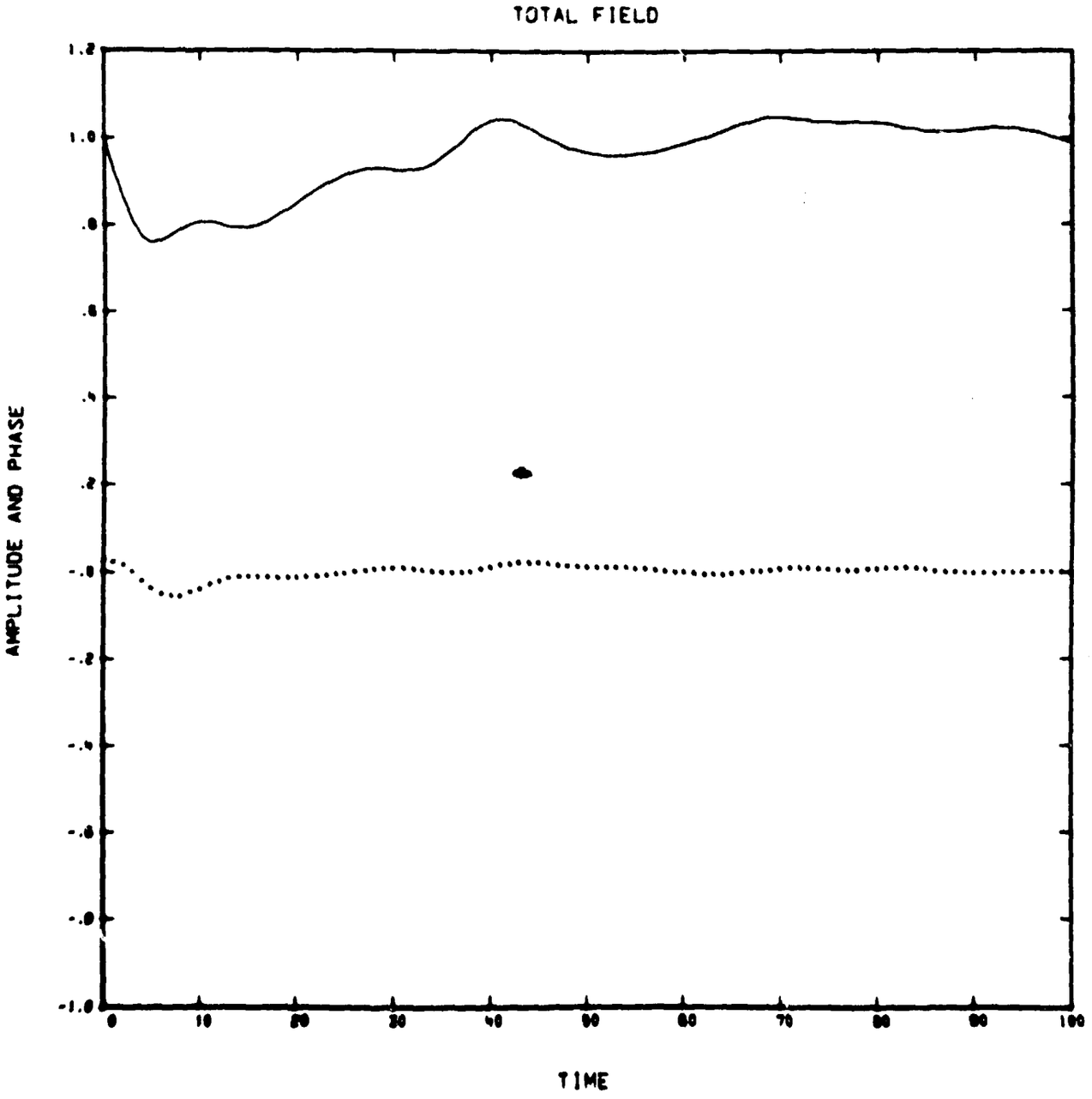
TOTAL FIELD
AMPLITUDE AND PHASE
TIME
1.2
1.0
.8
.6
.4
.2
-.0
-.2
-.4
-.6
-.8
-1.0
0
10
20
30
40
50
60
70
80
90
100

Fig. 9